Available online at www.sciencedirect.com
SCIENCE DIRECT
Mechatronics 16 (2006) 341–363
MECHATRONICS

Dynamic system identification and model-based fault diagnosis of an industrial gas turbine prototype

Silvio Simani [a,*], Cesare Fantuzzi [b,1]

[a] Dipartimento di Ingegneria, Università di Ferrara, Via Saragat 1, 44100 Ferrara, Italy
[b] Dipartimento di Scienze e Metodi per l'Ingegneria, Università di Modena e Reggio Emilia, Via Allegri 15, 42100 Reggio Emilia, Italy

Received 22 October 2004; accepted 18 January 2006

Abstract

In this paper, a model-based procedure exploiting analytical redundancy for the detection and isolation of faults on a gas turbine process is presented. The main point of the present work consists of exploiting system identification schemes in connection with observer and filter design procedures for diagnostic purpose. Linear model identification (black-box modelling) and output estimation (dynamic observers and Kalman filters) integrated approaches to fault diagnosis are in particular advantageous in terms of solution complexity and performance. This scheme is especially useful when robust solutions are considered for minimise the effects of modelling errors and noise, while maximising fault sensitivity. A model of the process under investigation is obtained by identification procedures, whilst the residual generation task is achieved by means of output observers and Kalman filters designed in both noise-free and noisy assumptions. The proposed tools have been tested on a single-shaft industrial gas turbine prototype model and they have been evaluated using non-linear simulations, based on the gas turbine data.

Keywords: Model-based fault diagnosis; Fault detection and isolation; Identification algorithms; Observer and Kalman filter design; Gas turbine

1. Introduction

The control devices currently in use to improve the overall performance of industrial processes involve both sophisticated digital system design techniques and complex hardware (sensors, actuators, processing units). The complexity means that the probability of fault occurrence can be significant and an automatic supervisory control system should be used to detect and isolate anomalous working conditions as early as possible.

This "early" detection and isolation of faults in engineering systems is a critical factor for avoiding product deterioration, loss of production, poor plant economy, performance degradation, major damage to machinery, environmental pollution and damage to human health or even loss of life.

These motivations pushed a great attention on fault detection and isolation (FDI) in dynamic processes the last two decades and a wide variety of so-called model-based approaches have been proposed to tackle this problem [39,32,6,40].

Model-based methods all use mathematical models of the plant being monitored. However, the conceptual realisation of these models can vary according to the following approaches: the parity space [21], state estimation [48,31,2,18,49,50], the fault detection filter [18,7,19], parameter identification [48,2,39,43,44,16] and non-linear techniques [36,14].

In each case, to guarantee that faults can be detected and isolated (and distinguishable), mathematical models of the process under investigation are required, either in state space or input–output form. State space descriptions generally provide mathematically rigorous tools for system

* Corresponding author. Tel./fax: +39 0532 97 4844.
E-mail addresses: silvio.simani@unife.it (S. Simani), cesare.fantuzzi@unimore.it (C. Fantuzzi).
[1] Tel.: +39 0522 522 213; fax: +39 0522 522 312.

0957-4158/$ - see front matter © 2006 Elsevier Ltd. All rights reserved.
doi:10.1016/j.mechatronics.2006.01.002

modelling and residual generation that may be used in fault detection of industrial systems, both for noise-free measurements and noisy data environment. Residuals should then be processed to detect an actual fault condition, rejecting any false alarms caused by noise or spurious signals. However, in practical applications, especially when considering large plants and complex systems, the straightforward application of such FDI techniques is difficult. In fact, the plant model is usually designed to carefully capture all kinds of details relevant to the analysis and the deployment of the real system. Thus, this model is often non-linear and very complex, and it can exploit look-up tables and hybrid structures to describes accurately the behaviour of the real target system. This intrinsic complexity, however, makes almost infeasible the straightforward application of cited FDI methods, and a viable procedure for practical application of FDI techniques is really necessary in complex applications.

In our view, the complexity of the accurate plant model can be somehow relaxed by reason of practical application to FDI schemes. In particular we investigated through a test-bed system the use of identification of linear models theory in the solution of fault detection and isolation problem. To this aim, we stressed two practical aspects in system identification which are of importance in FDI applications. Firstly, the system complexity may not indicate a requirement for a complex physical or thermodynamic model. In fact, as shown in this work, dynamic model identification methods for FDI can successfully be used, thus obviating the requirement for physical models. Therefore, a linear mathematical model (state-space or input–output descriptions) of the input–output links are obtained by means of identification schemes. In particular, when the signal to noise ratios are high, Auto Regressive eXogenous (ARX) models can be used. On the other hand, when the noise cannot be neglected, the Errors-In-Variables (EIV) models can be used, according to Kalman works [34,35]. Moreover, in the latter approach the identification technique is based on the rules of the Frisch scheme, based on traditional application to the analysis of economic systems [20]. These approaches provide a reliable model of the plant under investigation, as well as giving the variances of the input–output noises [5]. Both of these identification methods have been used in this work. Secondly, linear prototypes for the design of linear output estimators [44,43] have been developed instead of using non-linear models. This is considered important to avoid the complexities that would otherwise be inevitable when non-linear models are used. There is certainly an increasing interest in the use of non-linear methods (non-linear observers, extended Kalman filters, fuzzy-logic methods, etc.). However, as the feature of system supervision is to monitor the operation and performance of the system with respect to an expected point of operation, linear system methods are still very valid. Deviations from expected behaviour can be used to monitor system performance changes as well as component malfunctions. Moreover, the linear approach to fault diagnosis is still advantageous in terms of solution complexity and performance. This is especially true if so-called robust solutions are sought, where the robustness is used to minimise the effects of modelling errors.

This work concerns the use of methods that have this early FDI capability, long before the failure stage and before plant operation and safety are compromised. Faults at an early stage of development are referred to as incipient faults due to the inherent difficulty in detection and isolation. The presence of incipient faults is often unnoticeable in system measurements. This means that traditional methods are less likely to successfully detect and isolate incipient faults. We consider realistic data and measurements from a gas turbine rig. The main challenges are to provide a technology for signalling the onset of turbine faults before expensive failure occurs. It is our opinion that the methodology should be considered along with maintenance schedules with an aim to cut down maintenance cost, whilst steadily improving system reliability. The approach being evaluated has an important implication on the use of on-line FDI and diagnostic tools once the turbine is under customer operation. This work aims to define a comprehensive methodology for fault diagnosis by using an output estimation/filtering approach, in conjunction with residual processing schemes, including a simple threshold detection. This paper describes how this is achieved in noise-free measurement case and when the data are affected by noise, using statistical analysis tools. The complete procedures of model identification, residual generation and FDI have been tested on a single-shaft industrial gas turbine prototype. The work provides a description of extensive simulation results. Finally, the new aspect of the present work consists of exploiting identification schemes in connection with observer/filter design procedures for diagnostic purpose. In particular, linear model identification (black-box modelling) and output estimation (dynamic observers and Kalman filters) approaches to fault diagnosis are in particular advantageous in terms of solution complexity and performance. Moreover this characteristic is especially useful when *robust solutions* are considered, i.e. where the robustness is used to minimise the effects of modelling errors and to maximise fault sensitivity. As the feature of system diagnosis consists of monitoring the operating condition of the system with respect to an expected point of operation, linear system methods are very valid and effective. Any deviations from expected system behaviour (due to faults affecting the process inputs and outputs) could be used to monitor system performance changes as well as system component malfunctions.

The structure of the paper is the following. Basic assumptions about the fault model and monitored system are described in Section 2. The description of a general gas turbine prototype plant is outlined in Section 3. Hence, Section 4 presents the fault diagnosis problem as dynamic system identification and FDI integrated approach. In particular, Section 4.1 recalls dynamic system identification

methods suggested by the authors for the estimation of a suitable linear dynamic model of the monitored process. Section 4.2 presents the approach of residual generation with the aid of dynamic output observers and Kalman filters designed on the basis of the identified models. This section also shows the design of such estimators under the assumptions of both noise-free and noisy input–output data. Therefore, Section 5 shows how the proposed algorithms can be applied to the FDI of actuators, process components and input–output sensors of the industrial gas turbine process, described in Section 3. Results from simulation show that minimal detectable and isolable faults are perfectly compatible with the industrial target of this application. Finally, Section 6 summarises the contributions and achievements of the paper providing some suggestions for possible further research topics.

2. Model description

In the following it is assumed that the monitored system, depicted in Fig. 1, can be modelled in fault-free condition, by a linear, discrete-time, time-invariant, dynamic model in the form:

$$\begin{cases} \mathbf{x}(t+1) = \mathbf{A}\mathbf{x}(t) + \mathbf{B}\mathbf{u}^*(t), \\ \mathbf{y}^*(t) = \mathbf{C}\mathbf{x}(t), \quad t = 1, 2, \ldots \end{cases} \tag{1}$$

where $\mathbf{x}(t) \in \Re^n$ is the state vector, $\mathbf{y}^*(t) \in \Re^m$ the process output vector and $\mathbf{u}^* \in \Re^r$ the control input vector. $\mathbf{A}$, $\mathbf{B}$ and $\mathbf{C}$ are constant matrices of appropriate dimensions obtained by means of identification procedures proposed in the following.

Under fault-free conditions, the input and the output available sensor measurement signals $\mathbf{u}(t) = [u_1(t) \ldots u_r(t)]$ and $\mathbf{y}(t) = [y_1(t) \ldots y_m(t)]$ can be described by the following relations:

$$\begin{cases} \mathbf{u}(t) = \mathbf{u}^*(t) + \tilde{\mathbf{u}}(t), \\ \mathbf{y}(t) = \mathbf{y}^*(t) + \tilde{\mathbf{y}}(t). \end{cases} \tag{2}$$

In real applications, variables $\tilde{\mathbf{u}}(t)$ and $\tilde{\mathbf{y}}(t)$ represent noise signals which, due to technological reasons, may affect the behaviour of the input–output sensors.

The scheme shown in Fig. 1 describes the relations among the actual input sensors $\mathbf{u}^*(t)$ and $\mathbf{y}^*(t)$, the sensor faults $\mathbf{f}_u(t) = [f_{u_1}, \ldots, f_{u_r}]^{\mathrm{T}}$ and $\mathbf{f}_y(t) = [f_{y_1}, \ldots, f_{y_m}]^{\mathrm{T}}$ and the sensor outputs $\mathbf{u}(t)$ and $\mathbf{y}(t)$. These relations can be modelled by the following equations in the noise free case:

$$\begin{cases} \mathbf{u}(t) = \mathbf{u}^*(t) + \mathbf{f}_u(t), \\ \mathbf{y}(t) = \mathbf{y}^*(t) + \mathbf{f}_y(t). \end{cases} \tag{3}$$

Again according to Fig. 1, when *component faults* $\mathbf{f}_s(t) \in \Re^n$ can occur in the plant described by Eq. (1), the dynamic system will be modelled as

$$\mathbf{x}(t+1) = \mathbf{A}\mathbf{x}(t) + \mathbf{B}\mathbf{u}(t) + \mathbf{f}_s(t). \tag{4}$$

Faults $\mathbf{f}_c(t)$ can also occur on the regulator in the controller. In such a case, under the assumptions that $\mathbf{f}_u(t) = \mathbf{0}$ and $\mathbf{f}_y(t) = \mathbf{0}$, the link among the output $\mathbf{u}(t)$ of the regulator, its input $\mathbf{y}(t)$, and the controller faults $\mathbf{f}_c(t)$ can be modelled as

$$\mathbf{u}(t) = \tilde{\mathbf{u}}(t) + \mathbf{f}_c(t) + \mathbf{u}_R(t) \tag{5}$$

when the input–output behaviour of the controller (by neglecting its dynamics and assuming constant unitary gain) in the fault-free case can be described as

$$\mathbf{u}^*(t) = \mathbf{u}_R(t), \tag{6}$$

where $\mathbf{u}_R(t)$ represents the reference or set-point signal.

It is worthwhile stressing the difference between the fault signals $\mathbf{f}_u(t)$ and $\mathbf{f}_c(t)$. According to Eqs. (1) and (3), input sensor faults $\mathbf{f}_u(t)$ do not affect the monitored system (1). On the other hand, because of Eqs. (3) and (6), actuator (*or controller*) fault vector $\mathbf{f}_c(t)$ affects both the system of Eq. (1) and the vector $\mathbf{u}(t)$ by means of the signals $\mathbf{u}^*(t)$.

Usually $\mathbf{f}_u(t)$, $\mathbf{f}_y(t)$, $\mathbf{f}_s(t)$ and $\mathbf{f}_c(t)$ signals are described by step and ramp functions representing abrupt and incipient faults (bias or drift), respectively.

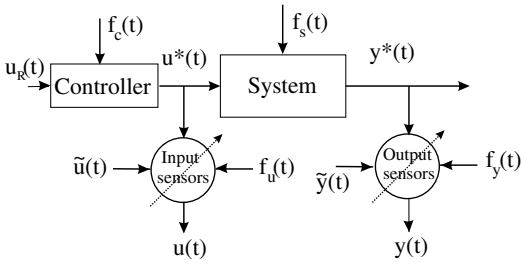

Fig. 1. The monitored system.

3. Modelling aspects of an industrial gas turbine prototype

This section describes the dynamic non-linear model of an industrial gas turbine as the presented metho methodology has aimed at the diagnosis of a wide range of components of an industrial process. The non-linear model has been calibrated by means of reference steady-state condition data of a real industrial gas turbine and it has been used to simulate various machine transient. Although the model is modular in structure and was carried out in simplified form, these features did not compromise its accuracy. The computation time is also minimal, making the modelling methods suitable for on-line simulation.

The comparison between values of working parameters obtained by the simulation and measurements during some transients on the gas turbine in operation provided encouraging results. The implementation of industrial gas turbine dynamic models can make it possible:

- to predict machine transient conditions due to component of different kind, volume and time constant, reducing test costs;
- to design gas turbine control systems;
- to generate time series of transient condition data.

In particular, it is possible to have a large volume of data otherwise difficulty to be available for industrial gas turbine that works mainly in steady-state conditions. In diagnostic applications, the machine dynamic model can be used to simulate operating conditions of gas turbines with faults in components, measurements and control sensors.

3.1. Gas turbine prototype model description

In this section, the model for simulating an industrial gas turbine, with variable compressor IGV angle and first turbine nozzle cooled alone, working in parallel with electric mains was carried out. More specific details regarding the description of the turbine main modules are also given in [45,43].

The dynamic non-linear gas turbine model has been developed by dividing the dynamic operation of the machine into elementary modules corresponding to its main components and developing a dynamic model for each of the modules. The overall representation of a specific gas turbine is carried out by identifying the necessary modules and connecting them appropriately by means of thermodynamic and mechanic links. The dynamic behaviour of each module is described by means of equations representing the thermodynamic transformations, the mass and momentum balance. The mass and momentum balance equations are used in one-dimensional differential form, in the hypothesis of assimilating each block to a constant section duct. Model equations are integrated considering that the change in the fluid density takes place according to an isentropic transformation. The equations representing the thermodynamic transformation are used instead in stationary form, since the fluid thermal inertia is considered negligible in comparison to the mechanical inertia.

From a mechanical standpoint, the fluid is considered as a perfect gas and in each modules are used mean values of specific heat at constant pressure and at a constant volume depending on the temperature between modules input and output and on the fluid composition. The use of mean specific heats in dynamic simulations, where the changes in thermodynamics and performance values are analysed with reference to an initial steady-state condition, does not significantly affect the result accuracy, but considerably reduces both the model complexity and the calculation time.

The mass flow rates bled on the compressor are calculated without considering the dynamic effects on them in transient conditions, and considering that the mass flow function of air bled at the outlet of each elementary compressor module is constant in all operating conditions. The effect on the thermodynamic cycle of turbine nozzle and blade row cooling flows, calculated starting from the mass flow rates bled on the compressor, is assessed by splitting the total cooling flow appropriately into two parts and assuming that one is mixed upstream and the other downstream from the turbine module, causing a reduction of the main flow total temperature and then, a reduction of the available enthalpy drop. In addition to the equations describing the various modules, equations are used that represent the dynamic balance of shafts and rotating masses of the machine connected to them. The simulation of the gas turbine working was carried out by integrating the differential equations and solving the static equations with the variable values calculated at each time instant.

Since the intention was to limit calculation and system costs in the subsequent diagnostic stage, it is necessary to be able to run the dynamic model on a PC using commercial available software. To achieve the integration of the differential equations SIMULINK© of MATLAB© [46,47] was used, as it is a feasible (easy to use) and wide spread software.

Fig. 2 represents the simplified block diagram of the machine and, in the following, Fig. 8 shows its schematic layout. These highlight boundary and control inputs and output variables, the compressor and turbine maps, direct and feedback main links among the various modules.

With reference to Fig. 2, M_f is the control input (fuel mass flow rate), whilst T_a, p_a (ambient temperature and pressure) and LHV (lower heating value) are boundary condition input, whilst P_e (electric power), T_5 and m_5 (turbine exhaust temperature and mass flow) are outputs.

The nomenclature used in Figs. 2 and 8 is described in Table 1.

The machine load adjustment is performed by means of fuel flow rate M_f control and varying the IGV angle with the logic of keeping the turbine outlet temperature constant. This logic is especially suited for optimum heat recovery steam generator operation in cogenerative applications. The SIMULINK© schemes of the speed controller of the turbine and of the pressurising valve model are sketched in Fig. 3.

To simulate this type of load control (by adjusting the IGV angle to keep the turbine outlet temperature constant) it was considered that the IGV angle at each time is obtained using a feedback PID controller applied to the turbine outlet temperature, as shown in Fig. 2.

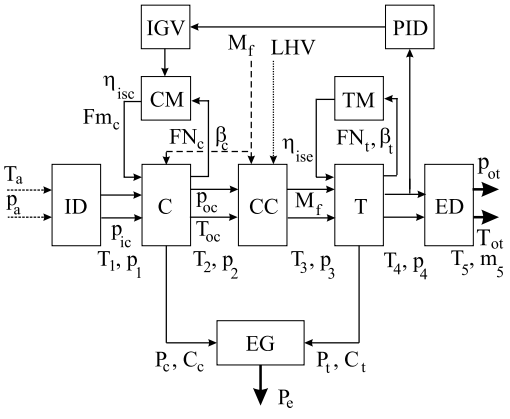

Fig. 2. Block diagram of the single-shaft gas turbine.

Table 1
Nomenclature

C	compressor
CC	combustor (combustion chamber)
CM	compressor map
ED	exhaust duct
EG	electric generator
ID	intake duct
IGV	inlet guide vanes
PID	proportional integral derivative controller
T	turbine
TM	turbine map
M_f	fuel mass flow rate
LHV	lower heating value
η_{isc}	isentropic compressor efficiency
Fm_c	compressor mass flow function
FN_c	compressor rotational speed function
β_c	compressor pressure ratio
η_{ise}	isentropic expansion efficiency
FN_t	turbine rotational speed function
β_t	turbine pressure ratio
t_i	ith section (module) temperature
p_i	ith section (module) pressure
m_i	ith section (module) mass rate
q_i	ith section (module) mass flow rate
T_a	ambient temperature
p_a	ambient pressure
P_c	compressor power
P_t	turbine power
C_c	compressor torque
C_t	turbine torque
P_e	electrical power
P_{ot}	turbine output pressure
w_t	turbine angular rate
N_t	turbine rotational speed
e_t	turbine efficiency
e_c	turbine efficiency

In order to assess the validity of the dynamic MATLAB/SIMULINK© model developed, it was decided to compare results obtained from the simulation of transient conditions with measurements taken on a gas turbine working in a cogeneration plant [45,43].

Load reduction transients on a single-shaft industrial gas turbine in operation were carried out by the control system in two ways:

- reducing the fuel flow rate M_f and closing the IGV to keep the turbine outlet temperature T_{ot} constant;
- reducing the fuel flow rate M_f alone, after that the IGV reached the total closer position.

As an example, for the first case, the electrical power P_e, the fuel flow rate M_f and the turbine outlet temperature T_{ot} during the transient were recorded.

The measurements for the first load reduction operation, corresponding to a specimen of the system dynamic behaviour, are shown in Figs. 4–6, in which a data sample is taken each 0.08 s. All data samples are normalised with respect to the standard deviation of the corresponding signals.

In the case examined, the PID control system characteristics were determined in order to reproduce, during the simulation, the electrical power P_e, the fuel flow rate M_f and the turbine outlet temperature T_{ot} experimentally recorded. In this way, the simulation provides the electrical power P_e, the fuel flow rate M_f and the turbine outlet temperature T_{ot} these variables are shown in Figs. 4–6 by using continuous lines. In the same figures, the estimated signals are then compared with the actual measurements acquired from the real process by sampling with regular time intervals (diamond symbols).

The agreement between the simulated and measured curves proves the validity of the dynamic MATLAB/SIMULINK© model developed and therefore shows how it is possible to reproduce the real behaviour of the process under investigation [45].

In particular, in the case of load reduction performed by the control system reducing the fuel flow rate and closing the IGV, the mean-square difference between the values obtained by the simulation and those measured experimentally are about 1.1% for the electrical power P_e, 10^{-3}% for fuel flow rate M_f and 0.4% for the turbine outlet temperature T_{ot}. Similarly, in the case of load reduction caused by the fuel flow rate M_f reduction, the mean-square differences are about 0.8% for the electrical power P_e and turbine outlet temperature T_{ot} whilst 0.4% for the fuel flow rate M_f. The percentage differences between calculated and measured transient final values are about 0.9% for the electrical power P_e, 0.001% for the fuel flow rate M_f and 0.5% for turbine outlet temperature T_{ot}, in the case of load reduction performed by fuel flow rate reduction and IGV closing. The percentage differences were about 0.6% for all three variables, in the case of load reduction caused by fuel flow rate reduction.

The above results confirms the validity of the gas turbine dynamic model. In particular, the developed simulator in MATLAB/SIMULINK© appears suitable for generating time series of transient condition data. Data sequences are exploited to derive the methodology for gas turbine operation monitoring and measurement and control sensors fault diagnosis.

3.2. Fault scenario description

Fault conditions are simulated using the turbine prototype developed in MATLAB/SIMULINK© environment. In particular, four fault cases have been considered in this work, namely:

(1) *Compressor contamination* (*system fault*), $f_s(t)$. The fault "case 1" represents fouling of the surfaces of the compressor blades, this reduces air flow, changes the blade aerodynamics and consequently changes the surface roughness. The failure is modelled as a gradual decrease in mass flow rate for a given pressure ratio. The maximum decrease in mass flow

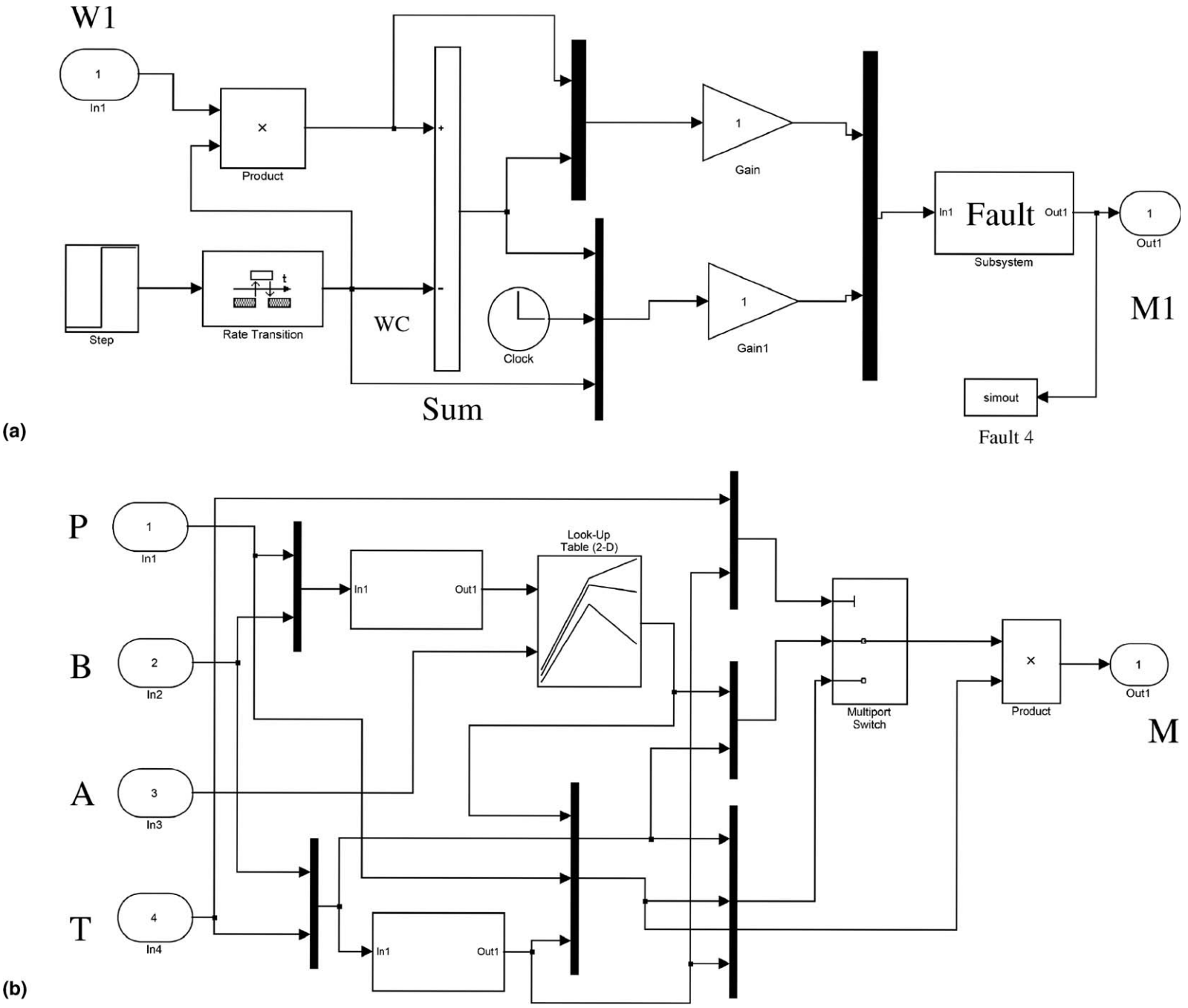

Fig. 3. SIMULINK© turbine (a) speed controller and (b) pressurising valve model.

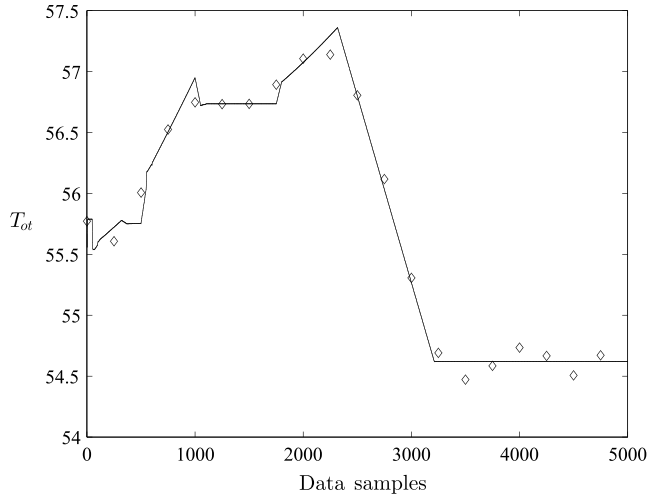

Fig. 4. Turbine outlet temperature T_{ot} in the case of load reduction performed reducing the fuel flow rate M_f and closing the IGV angle α.

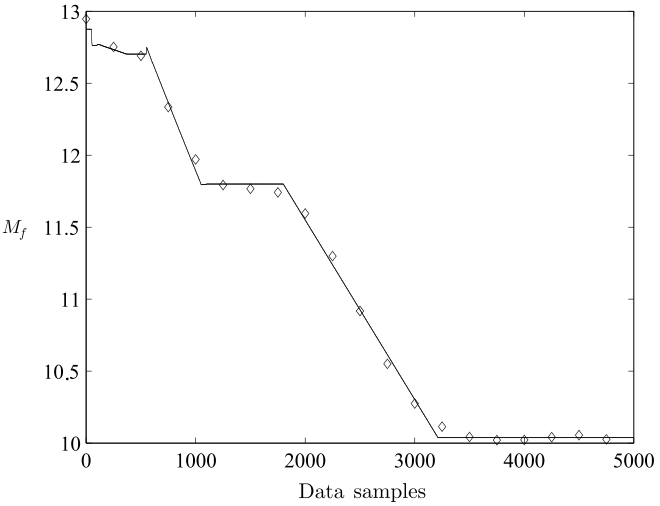

Fig. 5. Fuel flow rate M_f in the case of load reduction performed reducing the fuel flow rate M_f and closing the IGV angle α.

rate is set nominally at 5% while the fault development rate is set to (5% decrease of normal flow rate)/hour.

(2) *Thermocouple sensor fault* (*output sensor fault*), $f_y(t)$. The fault "case 2" represents the malfunctioning of a thermocouple in the turbine gas path which leads to a slowly increasing or decreasing reading over time. There is no limit placed on the error magnitude while the fault development rate is set to (5% error in measuring actual temperature)/hour.

(3) *Turbine damage* (*system fault*), $f_s(t)$. The fault "case 3" represents the fault $f_s(t)$ of the turbine. This results in a reduction in turbine efficiency. The fault $f_s(t)$ is modelled as a gradual reduction in turbine efficiency over time. The maximum decrease in turbine efficiency is set nominally at 5% while the fault development rate is set to (5% reduction of normal efficiency)/hour.

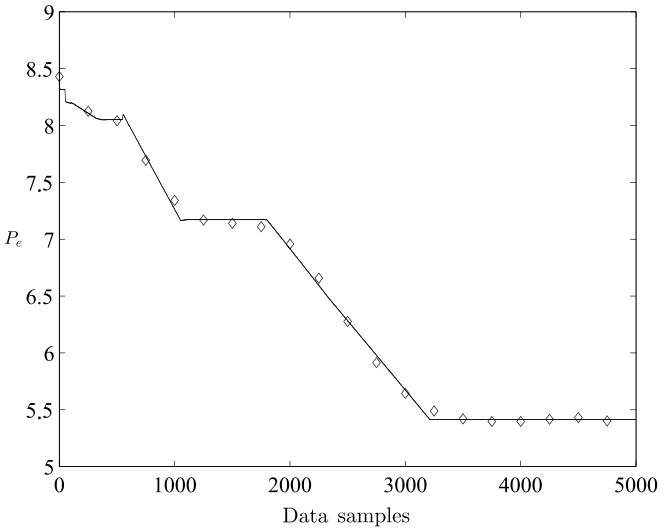

Fig. 6. Electrical power P_e in the case of load reduction performed reducing the fuel flow rate M_f and closing the IGV angle α.

(4) *Controller actuator fault* (*actuator fault*), $f_c(t)$. The fault "case 4" affects the actuator of the turbine controller. Under the assumption that there are no actuator dynamics in the current turbine model, the fault $f_c(t)$ of the actuator causes a slower response to demanded flow rates. Its effect is modelled as a simple first order lag on the resulting fuel flow. The actuator response time constant increases linearly with the time in order to represent a progressive damage to the actuator.

Note that in real industrial applications it is commonplace for each of the above faults to develop slowly over a period of months. For the purpose of this simulation, in order to avoid excessively long duration simulations, the fault development rate will be increased so that significant effects are present after 1 h. However, this is still considerably longer than the duration of the gas turbine dynamics which occur over periods of seconds, a factor which must be taken account of in any FDI algorithm design.

The rate of development and magnitude of faults have been set to nominal values in this case study. It will be of interest to know how small the fault parameters can be made whilst still maintaining good FDI performance. It is finally assumed that only a single fault may occur in the actuators, components or output sensors of the simulated plant.

3.3. Failure mode effect analysis (FMEA)

In order to understand the relations among injected fault signals and monitored measurements (e.g., q_l, t_k, p_h and m_j) from the turbine prototype, Table 2 shows the fault effect distribution in the case of a single fault occurrence in each actuator, component and sensor.

Table 2
Fault effect analysis

Fault/$y_i(t)$	q_l	t_k	p_h	m_j
Case 1	1	0	0	0
Case 2	0	1	0	0
Case 3	0	0	1	0
Case 4	0	0	0	1

Table 2 was obtained in noise-free conditions by performing a fault sensitivity analysis, i.e. by selecting the most sensitive output measurement $y_i(t)$ of $\mathbf{y}(t)$ with respect to the simulated generic fault case $f_y(t)$, $f_c(t)$ or $f_s(t)$.

The output measurements $\mathbf{y}(t)$ that are mainly affected by the considered fault situations are denoted by a '1' in the corresponding table entry, while an entry '0' means that the fault does not affect the correspondent output variable $y_i(t)$. Under these considerations, the entries '1's in Table 2 represent the output variables $\mathbf{y}(t)$ that are mainly sensitive to the considered fault case. It means that the sensitivity of the considered output measurement with respect to the concerning injected fault signal is greater than any other different fault cases. On the other hand, a '0' entry means that the effect of the fault on the considered output measurement can be neglected and therefore the considered fault does not affect the concerning output variable.

Note finally how faults occurring at the same time in actuator, components and sensor can be distinguished by analysing their effects on the monitored outputs $\mathbf{y}(t)$. This analysis allows also to simplify the identification procedure, as it reduces the number of output measurements $y_i(t)$ that have to be considered and monitored for the identification and FDI schemes.

4. Identification and FDI integrated approach

It is worth noting that the fault diagnosis scheme for the monitored process presented here requires the knowledge of a state-space model of the system under investigation. When classical modelling techniques cannot be used as the complete physical knowledge of the system is not available, the model is too complex, or the model parameters are not perfectly known, it is reasonable to consider a "black-box" identification approach [44,16] as suggested in this work. Therefore, next sections recalls briefly the problems of the identification (Section 4.1) and FDI (Section 4.2) of linear dynamic models in both the noise-free and noisy environment, respectively.

4.1. Dynamic linear model identification

4.1.1. ARX identification

In the first approach to identification presented here, no hypotheses about the input and output measurements acquired from the simulated process are assumed. In this situation, equation error (EE) identification can be exploited and, in particular, different EE models can be extracted from the data [44]. A specific discrete-time, time-invariant, linear dynamic model, e.g., ARX (Auto Regressive eXogenous) [37,43], can be selected inside the assumed family of models.

Hence, the input–output link can be mathematically described by performing the identification of a multiple-input multiple-output (MIMO) input–output minimal parameterisation models of the type:

$$y_i(t+\nu_i) = \sum_{j=1}^{m}\sum_{k=1}^{\nu_{ij}} \alpha_{ijk}\mathbf{y}_j(t+k-1) + \sum_{j=1}^{r}\sum_{k=1}^{\nu_i} \beta_{ijk}\mathbf{u}_j(t+k-1), \tag{7}$$

where the integers ν_i $(i=1,\ldots,m)$ are related to the structure of the model and define the order n of the system and its memory as

$$n = \sum_{i=1}^{m} \nu_i. \tag{8}$$

The integers ν_{ij} appearing in Eq. (7) are univocally defined by the structure of the model through the relations:

$$\begin{cases} \nu_{ij} = \nu_i & \text{for } i = j, \\ \nu_{ij} = \min(\nu_i + 1, \nu_j) & \text{for } i > j, \\ \nu_{ij} = \min(\nu_i, \nu_j) & \text{for } i < j. \end{cases} \tag{9}$$

The model in the form of Eq. (7), can also be rewritten by means of an input–output equivalent polynomial form:

$$\mathbf{P}(z)\mathbf{y}(t) = \mathbf{Q}(z)\mathbf{u}(t), \tag{10}$$

where z denotes the unitary advance operator, $\mathbf{P}(z)$, $\mathbf{Q}(z)$ are polynomial matrices in canonical form [24,3,25]. The entries of $\mathbf{P}(z)$ and $\mathbf{Q}(z)$ are given by

$$\begin{aligned} p_{ii}(z) &= z^{\nu_i} - \alpha_{ii\nu_i} z^{(\nu_i-1)} - \cdots - \alpha_{ii2}z - \alpha_{ii1}, \\ p_{ij}(z) &= -\alpha_{ij\nu_{ij}} z^{(\nu_{ij}-1)} - \cdots - \alpha_{ij2}z - \alpha_{ij1}, \\ q_{ij}(z) &= \beta_{ij\nu_i} z^{(\nu_i-1)} + \cdots + \beta_{ij2}z + \alpha_{ij1}. \end{aligned} \tag{11}$$

The model structure, i.e. the order n and the parameter vectors α_{ijk}, β_{ijk} of the polynomials in the matrices $\mathbf{P}(z)$, $\mathbf{Q}(z)$ of the model have to be determined by an identification approach [27,24,3,25]. The signal $y_i(t)$ in Eq. (7) or $\mathbf{y}(t)$ in Eq. (10) represents the one-step-ahead prediction for the actual ith output measurements $\mathbf{y}(t)$ [37].

If $\theta = \{\alpha_{ijk}, \beta_{ijk}\}$, $\nu = (\nu_1, \ldots, \nu_m)$ and $J(\theta, \nu)$ a selected cost function, the problem of identifying a multivariable model can be described as the determination, on the basis of given input–output sequences, of a suitable structure ν and parameters θ minimising $J(\theta, \nu)$. The cost function $J(\theta, \nu)$ can be described as, e.g., the PPCRE criteria[2] [28],

[2] PPCRE (predicted per cent reconstruction error) is defined as $\text{PPCRE}\% = 100 \times \frac{\text{stddev}(y-\hat{y})}{\text{stddev}\, y}$.

or AIC, MDL tests [37], connected to the prediction error of the identified model.

4.1.2. EIV identification

The second approach of this study to system identification considers the situation in which the input–output data acquired from the process under investigation can be affected by additive noise.

Therefore, under this assumption, the so-called Frisch scheme [20] is considered by the authors and applied to perform the dynamic system identification. Such a scheme allows to determine the linear discrete system which has generated the noisy sequences $\{\mathbf{u}(t), \mathbf{y}(t)\}$ as well as the variances of the noise signals $\{\tilde{\mathbf{u}}(t), \tilde{\mathbf{y}}(t)\}$ now corrupting the data [5].

In the ideal Frisch scheme these signals usually are assumed zero-mean white noises, mutually uncorrelated and uncorrelated with every component of $\mathbf{u}^*(t)$ and $\mathbf{y}^*(t)$. Moreover, it is normally assumed that:

$$\begin{cases} \mathbf{u}(t) = \mathbf{u}^*(t) + \tilde{\mathbf{u}}(t), \\ \mathbf{y}(t) = \mathbf{y}^*(t) + \tilde{\mathbf{y}}(t), \end{cases} \tag{12}$$

where every noise signals $\tilde{\mathbf{u}}(t)$ and $\tilde{\mathbf{y}}(t)$ are independent of every other term $\mathbf{u}(t)$ and $\mathbf{y}(t)$ only.

In the present noisy case, the identification problem can therefore be solved [5] by determining, if possible, the order n and the parameter vectors α_{ijk} and β_{ijk} of a model described by Eq. (7), as well as the variances of the input–output additive noise of Eq. (12). In fact, given the noisy input–output sequence $\{\mathbf{u}(t), \mathbf{y}(t)\}$, the recalled identification scheme provides the model which has generated the noiseless sequences $\{\mathbf{u}(t), \mathbf{y}(t)\}$ [29,13]. It is interesting to note that the relations given by Eqs. (10) and (12) describes the so-called Errors-In-Variables (EIV) models [34,35,5,4].

The next step is the transformation of the input–output, discrete-time, time-invariant canonical polynomial model of Eq. (10) into its canonical state-space representation [25]. In this context, as the FDI task is performed by means of output estimators (see next Section 4.2), the authors suggest to use the state-space canonical systems obtained by the EE models for designing dynamic observers [44,43], whilst the EIV coming from the Frisch scheme [44,16], in order to build Kalman filters, as shown in [29,13]. In particular for the latter approach, it is worthwhile underlining that the problem of identifying EIV models from noisy input–output sequences is considered in particular with reference to filtering applications and design, with reference to the "EIV optimal filtering" problem [29,13].

It is important to note that in the case of a MIMO linear model, the possible choice of state-space representations (of input–output ARX and EIV models) in canonical form [24,25] instead of parity space methods [21] (in connection with input–output linear prototypes) may avoid unexpected false alarm problems [11].

Finally, once the parameters $\theta = \{\alpha_{ijk}, \beta_{ijk}\}$ and the structure $\nu = (\nu_1, \ldots, \nu_m)$ have been identified, the link between canonical state-space $(\mathbf{A}, \mathbf{B}, \mathbf{C})$ and input–output $(\mathbf{P}, \mathbf{Q})$ models can be described by the following relations:

$$\mathbf{A} = [\mathbf{A}_{ij}] \tag{13}$$

with

$$\mathbf{A}_{ii} = \begin{bmatrix} 0 & 1 & \ldots & 0 \\ \vdots & \vdots & \ddots & \vdots \\ 0 & 0 & \ldots & 1 \\ \alpha_{ii1} & \alpha_{ii2} & \ldots & \alpha_{ii\nu_i} \end{bmatrix}_{(\nu_i \times \nu_i)}, \tag{14}$$

$$\mathbf{A}_{ij} = \begin{bmatrix} 0 & \ldots & \ldots & \ldots & \ldots & 0 \\ \vdots & & & & & \vdots \\ 0 & \ldots & \ldots & \ldots & \ldots & 0 \\ \alpha_{ij1} & \ldots & \alpha_{ij\nu_{ij}} & 0 & \ldots & 0 \end{bmatrix}_{(\nu_i \times \nu_j)} \tag{15}$$

and

$$\mathbf{C} = \begin{bmatrix} 1 & 0 & \ldots & \ldots & \ldots & \ldots & \ldots & \ldots & \ldots & 0 \\ 0 & \ldots & 0 & 1 & 0 & \ldots & \ldots & \ldots & \ldots & 0 \\ \vdots & \ldots & \ldots & \ldots & \ldots & \ldots & \ldots & \ldots & \ldots & \vdots \\ 0 & \ldots & \ldots & \ldots & \ldots & 0 & 1 & 0 & \ldots & 0 \end{bmatrix}, \tag{16}$$

where the 1's entries in the matrix $\mathbf{C}$ are in the columns $1, (\nu_i + 1), \ldots, (\nu_1 + \cdots + \nu_{m-1} + 1)$.

Moreover, the input distribution matrix $\mathbf{B}$ can be computed as

$$\mathbf{B} = \mathbf{M}^{-1}\overline{\mathbf{B}}, \tag{17}$$

where

$$\overline{\mathbf{B}} = \begin{bmatrix} \overline{\mathbf{B}}_1 \\ \overline{\mathbf{B}}_2 \\ \vdots \\ \overline{\mathbf{B}}_m \end{bmatrix}, \quad \overline{\mathbf{B}}_i = \begin{bmatrix} \beta_{i11} \ldots \beta_{ir1} \\ \vdots \ddots \vdots \\ \beta_{i1\nu_i} \ldots \beta_{ir\nu_i} \end{bmatrix}, \tag{18}$$

and

$$\mathbf{M} = [\mathbf{M}_{ij}], \quad \text{with } i, j = 1, \ldots, m, \tag{19}$$

where

$$\mathbf{M}_{ii} = \begin{bmatrix} -\alpha_{ii2} & -\alpha_{ii3} & \ldots & -\alpha_{ii\nu_i} & 1 \\ -\alpha_{ii3} & -\alpha_{ii4} & \ldots & 1 & 0 \\ \vdots & \vdots & & & \vdots \\ -\alpha_{ii\nu_i} & 1 & & & \vdots \\ 1 & & & & \end{bmatrix}_{(\nu_i \times \nu_i)} \tag{20}$$

and

$$\mathbf{M}_{ij} = \begin{bmatrix} -\alpha_{ii2} & -\alpha_{ii3} & \dots & -\alpha_{iiv_{ij}} & 0 \\ -\alpha_{ii3} & -\alpha_{ii4} & \dots & 0 & 0 \\ \vdots & \vdots & & & \vdots \\ -\alpha_{iiv_{ij}} & 0 & & & 0 \\ 0 & \dots & \dots & \dots & 0 \\ 0 & \dots & \dots & \dots & 0 \end{bmatrix}_{(v_i \times v_j)} . \tag{21}$$

It is worth noting that the bijection defined by the matrix $\mathbf{M}$ between the entries of $\mathbf{P}(z)$ polynomial matrix and $\mathbf{B}$ is always well-conditioned, with $|\det(\mathbf{M})| = 1$, independently of the actual values of the scalars α_{ijk} [26]. Moreover, because of the invertibility of $\mathbf{M}$, the bijective transformation holds between canonical state-space purely dynamic system $(\mathbf{A}, \mathbf{B}, \mathbf{C})$ and input–output polynomial model $(\mathbf{P}, \mathbf{Q})$. These models are therefore characterised by the same minimal numbers of parameters.

4.2. Residual generation

As depicted in Fig. 7, the symptom (or residual $\mathbf{r}(t)$) generation is implemented by means of dynamic observers or Kalman filters, driven by the measured sequences $\mathbf{u}(t)$ and $\mathbf{y}(t)$. Moreover, by means of these devices, due to the structure of the $\mathbf{C}$ matrix (see relation of Eq. (16)) and because of the fault affects analysed in Section 3.3, a set of signals can be produced from which it will be possible to isolate faults associated to actuators, components and sensors. On the other hand, the symptom evaluation refers to a logic device which processes the redundant signals generated by the first block in order to estimate and unequivocally identify a fault occurrence.

With reference to Fig. 7 the symptom signals are differences between estimated signals (given by observers or Kalman filters) and the actual ones supplied by the input and output sensors.

As stated in the previous section, the banks of output observers and Kalman filters are used when EE and EIV models are considered, respectively.

In particular, the dynamic observers for the system of the form of Eq. (1) have the following structure:

$$\begin{cases} \hat{\mathbf{x}}(t+1) = \mathbf{A}\hat{\mathbf{x}}(t) + \mathbf{B}\mathbf{u}(t) + \mathbf{K}(\mathbf{y}(t) - \mathbf{C}\hat{\mathbf{x}}(t)), \\ \hat{\mathbf{y}}(t) = \mathbf{C}\hat{\mathbf{x}}(t), \end{cases} \tag{22}$$

$\hat{\mathbf{x}}(t)$ being the estimate of the observer state vector, $\hat{\mathbf{y}}(t)$ the estimate of the measured outputs $\mathbf{y}(t)$, whilst the triple $(\mathbf{A}, \mathbf{B}, \mathbf{C})$ is a minimal state-space canonical representation describing the identified input–output model of Eq. (10) from the inputs to the outputs of the process.

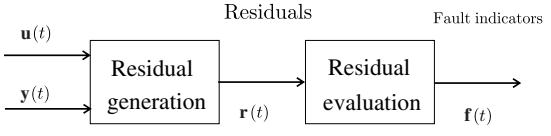

Fig. 7. Logic diagram of the fault detection system.

The observer eigenvalues, $\mathbf{p} = [p_1, \dots, p_n]$, placed on the basis of the gain matrix $\mathbf{K}$, are chosen inside the positive unit circle by solving the minimisation problem:

$$\min_{\mathbf{p}} V(\mathbf{p}). \tag{23}$$

$V(\mathbf{p})$ being the cost function described by the formula:

$$V(\mathbf{p}) = \frac{\sum_t r^2(t,\mathbf{p})|_h}{\sum_t r^2(t,\mathbf{p})|_f} = \frac{\|r(t,\mathbf{p})|_h\|^2}{\|r(t,\mathbf{p})|_f\|^2}, \tag{24}$$

where $\|\cdot\|$ represents the 2-norm or the mean square value of the vector $r(\cdot)$, i.e. the square root of the sum of the squared entries of the vector $r(\cdot)$. The residual signal $r(t,\mathbf{p})$ is a function of the vector $\mathbf{p}$, as the observer gain matrix $\mathbf{K}$ depends on the placement of the eigenvalues $\mathbf{p}$.

Hence, according to Eq. (23), eigenvalues $\mathbf{p} = [p_1, \dots, p_n]$ are chosen in order to maximise the mean square error of the fault residual sensitivity $r(t,\mathbf{p})|_f$ and minimise the mean square error of the residual in fault-free condition, $r(t,\mathbf{p})|_h$. This pole placement procedure provides robustness property versus modelling error to the observer and, consequently, false alarm rejection.

In particular, the residual vectors are described by the relations:

$$\begin{cases} r(t,\mathbf{p})|_h = \mathbf{y}(t) - \mathbf{C}\hat{\mathbf{x}}(t,\mathbf{p}) & \text{in fault-free conditions} \\ r(t,\mathbf{p})|_f = \mathbf{y}(t) - \mathbf{C}\hat{\mathbf{x}}(t,\mathbf{p}) & \text{in faulty conditions} \end{cases}$$

that can be rewritten as

$$\begin{cases} r(t,\mathbf{p})|_h = \mathbf{y}(t) - \mathbf{C}[z\mathbf{I} - (\mathbf{A} - \mathbf{KC})]^{-1} \times [\mathbf{B}\mathbf{u}(t) + \mathbf{K}\mathbf{y}(t)] \\ \qquad \text{in fault-free conditions i.e. } \mathbf{f}_u(t) = \mathbf{0}, \\ \qquad \mathbf{f}_y(t) = \mathbf{0},\ \mathbf{f}_s(t) = \mathbf{0} \text{ and } \mathbf{f}_c(t) = \mathbf{0} \\ r(t,\mathbf{p})|_f = \mathbf{y}(t) - \mathbf{C}[z\mathbf{I} - (\mathbf{A} - \mathbf{KC})]^{-1} \\ \qquad \times [\mathbf{B}\mathbf{u}(t) + \mathbf{K}\mathbf{y}(t) + \mathbf{B}\mathbf{f}_u(t) + \dots + \mathbf{B}\mathbf{f}_c(t) \\ \qquad + \mathbf{f}_s(t) + \mathbf{K}\mathbf{f}_y(t)] - \mathbf{f}_y(t) \\ \qquad \text{in faulty conditions i.e. } \mathbf{f}_u(t) \neq \mathbf{0}, \\ \qquad \mathbf{f}_y(t) \neq \mathbf{0},\ \mathbf{f}_s(t) \neq \mathbf{0} \text{ and } \mathbf{f}_c(t) \neq \mathbf{0} \end{cases} \tag{25}$$

where z is the unitary advance operator, whilst the fault vectors $\mathbf{f}_u(t)$, $\mathbf{f}_y(t)$, $\mathbf{f}_s(t)$ and $\mathbf{f}_c(t)$ are defined by Eqs. (3)–(5), depending on the considered fault case. The signals $\mathbf{u}(t)$ and $\mathbf{y}(t)$ represent the fault-free input and output vectors acquired from the actual process, respectively, as described in Section 2.

The problem given by relation of Eq. (23) can be solved in MATLAB© environment by means of the *Optimisation Toolbox* [46] using, e.g., the constrained minimisation functions `FMINCON`, `CONSTR` and `LEASTSQ`. These numerical routines used to solve the pole placement optimisation can allow to obtain stable observers in the form of Eq. (22). It can be successfully used also the *Genetic Algorithm*

Optimisation Toolbox of MATLAB©, that seems able to manage the well-known problems of local minima.

The evaluation of the cost function of Eq. (24) leads to the optimisation problem that can be sketched by the Algorithm 1 below. The solution obviously depends on the experimental conditions, as the values of the cost function of Eq. (24) are computed on the basis of the non-linear process input–output sequences.

Algorithm 1.

Step 1: initial estimate for the observer eigenvalues $\mathbf{p}$;
Step 2: fault-free input–output $\hat{\mathbf{u}}(t), \hat{\mathbf{y}}(t)$ sequence generation;
Step 3: fault-free residual vector $r(t,\mathbf{p})|_h$ computation (Eq. (25));
Step 4: faulty input–output $\hat{\mathbf{u}}(t), \hat{\mathbf{y}}(t)$ sequence generation;
Step 5: faulty residual vector $r(t,\mathbf{p})|_f$ computation (Eq. (25));
Step 6: cost function $V(\mathbf{p})$ of Eq. (24) evaluation;
Step 7: eigenvalues $\mathbf{p}$ variation along the direction of the function $V(\mathbf{p})$ decrease;
Step 8: `goto` Step 2.

It is worth noting that optimisation algorithms exploited for implementing Algorithm 1 should find a constrained (poles search inside the unit circle) minimum of a scalar function of several variables starting at an initial estimate. This is generally referred to as constrained non-linear optimisation or non-linear programming.

They are based on numerical optimisation algorithms. As an example, the optimisation function exploits a "Large-Scale" optimisation method. By default the optimisation function chooses the large-scale algorithm when the gradient of the optimised function is provided and if only upper and lower bounds exist or only linear equality constraints exist. This algorithm consists of a subspace trust region method and is based on the "interior-reflective Newton method" described in [10,9]. Each iteration involves the approximate solution of a large linear system using the method of preconditioned conjugate gradients (PCG). For more details, see the trust-region and preconditioned conjugate gradient method descriptions in [38].

On the other hand, if the"Medium-Scale" optimisation is considered, a sequential quadratic programming (SQP) method is used. In this method, a quadratic programming (QP) subproblem is solved at each iteration. An estimate of the Hessian of the Lagrangian is updated at each iteration using the BFGS formula [17,23]. A line search is performed using a merit function similar to that proposed by Han [30], Powell [42,41]. The QP subproblem is solved using an active set strategy similar to that described in [22].

Roughly speaking, in the absence of faults, the residual signals $r(t) = \mathbf{y}(t) - \mathbf{C}\hat{\mathbf{x}}(t)$ should be approximately zero. Hence, the symptom evaluation is obtained simply by comparing residual signals $r(t)$ with a fixed threshold ϵ according to the following geometric test:

$$\begin{cases} |r(t)| \leqslant \epsilon & \text{for } \mathbf{f}(t) = \mathbf{0}, \\ |r(t)| > \epsilon & \text{for } \mathbf{f}(t) \neq \mathbf{0} \end{cases} \tag{26}$$

$\mathbf{f}(t)$ being a generic fault vector. It is worth noting that, the term ϵ can describe an adaptive thresholds $\epsilon(t)$ which depend on plant operating conditions and $\epsilon(t)$ values have to be computed as function of plant inputs [8,6]. A FDI technique with the threshold adaptor or selector is described also in [15,12]. This method represents a passive approach since no effort is made to design a robust residual.

On the other hand, regarding the noisy case, with reference to the fault-free system, described by a minimal state-space EIV model $(\mathbf{A},\mathbf{B},\mathbf{C})$ given by Eqs. (10) and (12), a Kalman filter has the structure [29,13]:

$$\begin{cases} \hat{\mathbf{x}}(t+1|t) = \mathbf{A}\hat{\mathbf{x}}(t|t-1) + \mathbf{B}\mathbf{u}(t) \\ \qquad\qquad + \mathbf{K}(t)(y(t) - \mathbf{C}\hat{\mathbf{x}}(t|t-1)), \\ \hat{y}(t|t) = \mathbf{C}(\mathbf{I} - \mathbf{K}(t)\mathbf{C})\hat{\mathbf{x}}(t|t-1) + \mathbf{C}\mathbf{K}(t)y(t). \end{cases} \tag{27}$$

The variable $\hat{\mathbf{x}}(t+1|t)$ represents the one step ahead prediction of the system state of Eq. (4), whilst the signal $\hat{y}(t|t)$ is the estimate of the output $\mathbf{y}(t)$ given by the filter.

A Riccati equation is used to compute the time-variant gain $\mathbf{K}$ of the filter by means of the knowledge of the covariance matrix of the input vector noise $\tilde{\mathbf{u}}(t)$ and the variance of the ith component of the output noise $\tilde{\mathbf{y}}(t)$, obtained from the application of the Frisch scheme methodology, as shown in [29,13].

It can be proved [33] that the innovation signal $r(t) = \mathbf{y}(t) - \mathbf{C}\hat{\mathbf{x}}(t|t-1)$ is a white process when all the assumptions regarding the system $(\mathbf{A},\mathbf{B},\mathbf{C})$ and the statistical characteristics of the noises are completely fulfilled. In particular, the innovation converges to a steady state solution when the pair $(\mathbf{A},\mathbf{B})$ is completely reachable and the pair $(\mathbf{A},\mathbf{C})$ is completely observable.

Because of the linear property of system of Eq. (2) and because of the effect of faults on the system output measurements, any change in measurements due to a fault is reflected in a change in the mean and in the standard deviation of $r(t)$, therefore the detection strategy which is commonly chosen in connection with Kalman filtering methods for failures detection consists in monitoring the innovations $r(t)$. In particular, since the Kalman filter produces zero-mean and independent white residuals with the system in normal operation, a method for failure detection and isolation consists in testing how much the sequence of innovations has deviated from the white noise hypothesis. The tests which can be performed on the innovations are the usual ones for zero-mean and variance, as cumulative sum algorithms as well as independence, as χ^2-type. If a system abnormality occurs, the statistics of $r(t)$ change, so its comparison with a threshold fixed under no faults conditions, becomes the detection rule.

It is assumed that only a single fault may be present in the actuators, components or input sensors of the plant at any given time. On the other hand, in some cases the

proposed methodology can effectively handle multiple faults.

It is worth noting that the new aspect of the present work consists of exploiting identification schemes in connection with observer/filter design procedures for diagnostic purpose. In particular, linear model identification (black-box modelling) and output estimation (dynamic observers and Kalman filters) approaches to fault diagnosis are in particular advantageous in terms of solution complexity and performance. Moreover this characteristic is especially useful when *robust solutions* are considered, i.e. where the robustness is used to minimise the effects of modelling errors and to maximise fault sensitivity. As the feature of system diagnosis consists of monitoring the operating condition of the system with respect to an expected point of operation, linear system methods are very valid and effective. Any deviations from expected system behaviour (due to faults affecting the process inputs and outputs) could be used to monitor system performance changes as well as system component malfunctions.

5. Identification and FDI of the gas turbine prototype

The following sections show the complete design procedure for a model-based fault diagnosis system, starting from system identification, both in the noise-free and noisy environment, to residual generation for fault detection and isolation. The procedure is applied to a model of a real industrial plant [45].

Two points have to be underlined here. Firstly, Section 5.1 describes how linear state-space models have been identified for principal working conditions of the plant, as state-space descriptions provide general and mathematically rigorous tools for system modelling and residual generation that may be used successfully for fault diagnosis. Secondly, Sections 5.2 and 5.7 show how residuals should then be processed to detect an actual fault condition, rejecting any false alarms caused by noise or spurious signals. In particular, this work addresses output estimation approach for fault diagnosis of actuators, components and input–output sensors, mainly in conjunction with residual processing schemes which include a simple threshold detection [6] as well as residual statistical analysis.

Moreover, one of the main reasons of the proposed methodology should be stressed again. Linear prototypes for the design of linear output estimators [44] have been identified here instead of non-linear models obtained by modelling techniques in connection with non-linear observers. In fact, in some cases, the linear approach is still advantageous in terms of solution complexity and performance. Moreover linear system methods are still very valid since the feature of the system supervision is to monitor the operation and performance of the system with respect to an expected point of operation. It must be realised that, of course, a change in point of operation can be indicative of a fault in the process.

5.1. Dynamic process identification

The identification procedure presented in Section 4.1 has been applied to the industrial gas turbine prototype developed in MATLAB/SIMULINK© environment described in Section 3.1 [45]. It is a strongly non-linear model, as it consists mainly of non-linear functions and look-up tables that model the thermodynamic relations among the variables involved.

Fig. 8 shows the block schematic diagram of the gas turbine including its inputs and outputs.

Air flows (ambient air temperature and pressure, p_a and T_a, that are not control inputs) via an inlet duct to the compressor (“compressor” block), high pressure air from the compressor is heated in combustion chambers (“combustor” block) and expands through a single stage compressor turbine (“turbine” block). A butterfly valve (valve angle, a_v) provides a means of controlling the speed of the turbine (first control input, $u_1(t)$). Cooling air is bled from the compressor outlet to cool the turbine stator and rotor.

A regulator (“controller” block) regulates the combustor fuel flow (M_f in Fig. 8) to maintain the compressor speed (N_t) at a set-point value. Under steady state conditions, the power generated by the turbine is balanced by that absorbed by the compressor and losses since there is no power turbine present in the model.

The process inputs $u_i(t)$ are the ambient air temperature T_a and pressure p_a, fuel flow $M_f(u_2(t))$ and the butterfly valve opening angle $(a_v, u_1(t))$. As an example, the control input signals $a_v(t)$ and $M_f(t)$, as well as the boundary condition inputs T_a and pressure p_a are shown in Fig. 9. Note that the input signals are also affected by the measurement noise, whose levels are reported in Table 4.

The process outputs $y_i(t)$ consist of all the 28 measurements that can be acquired from each block of the simulated MATLAB/SIMULINK© system, e.g., mass flow (m_j), temperature (t_k), pressure (p_h), torque (q_l) and speed (N_t) signals.

It is worth noting that, according to Section 3.3, among the 28 output measurements, q_l, t_k, p_h and m_j only have to be monitored for the identification and FDI schemes presented here.

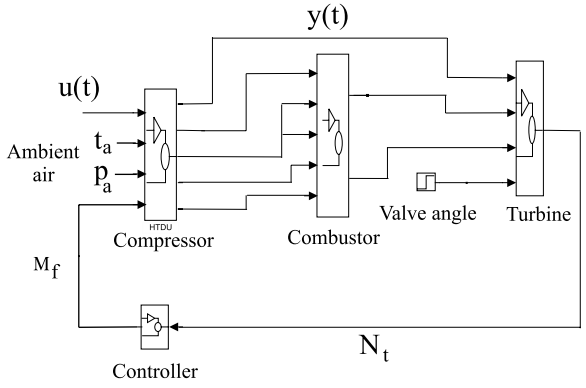

Fig. 8. The monitored turbine process.

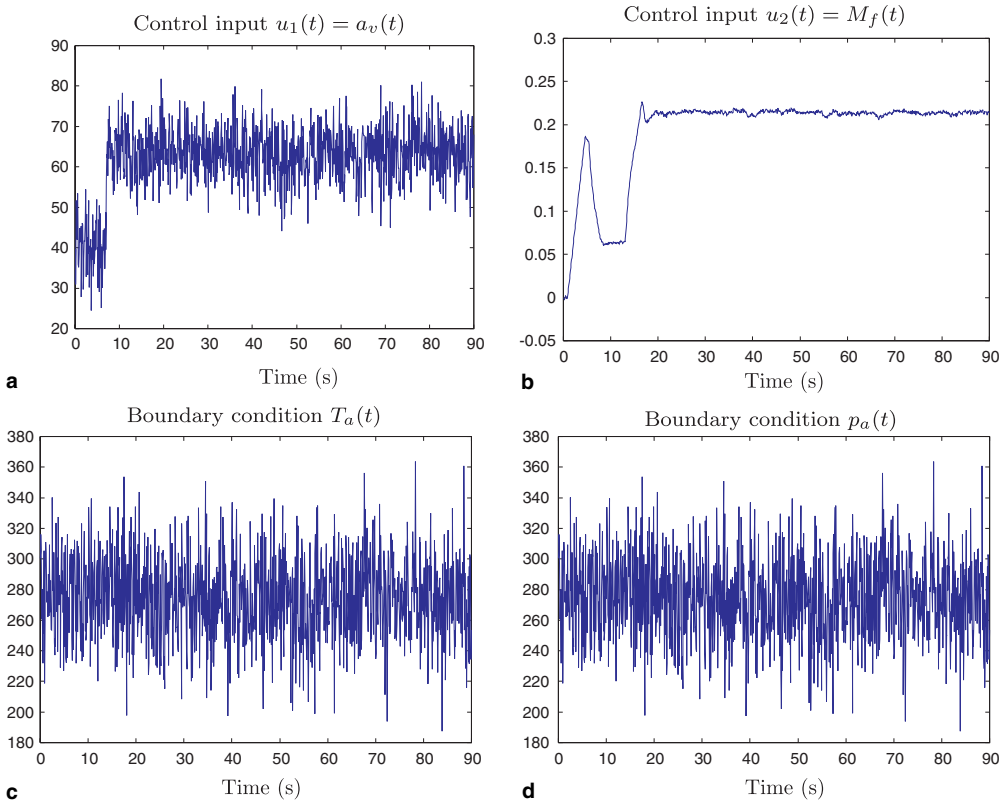

Fig. 9. Gas turbine input signals: (a) valve angle, (b) fuel flow, (c) ambient temperature and (d) ambient pressure.

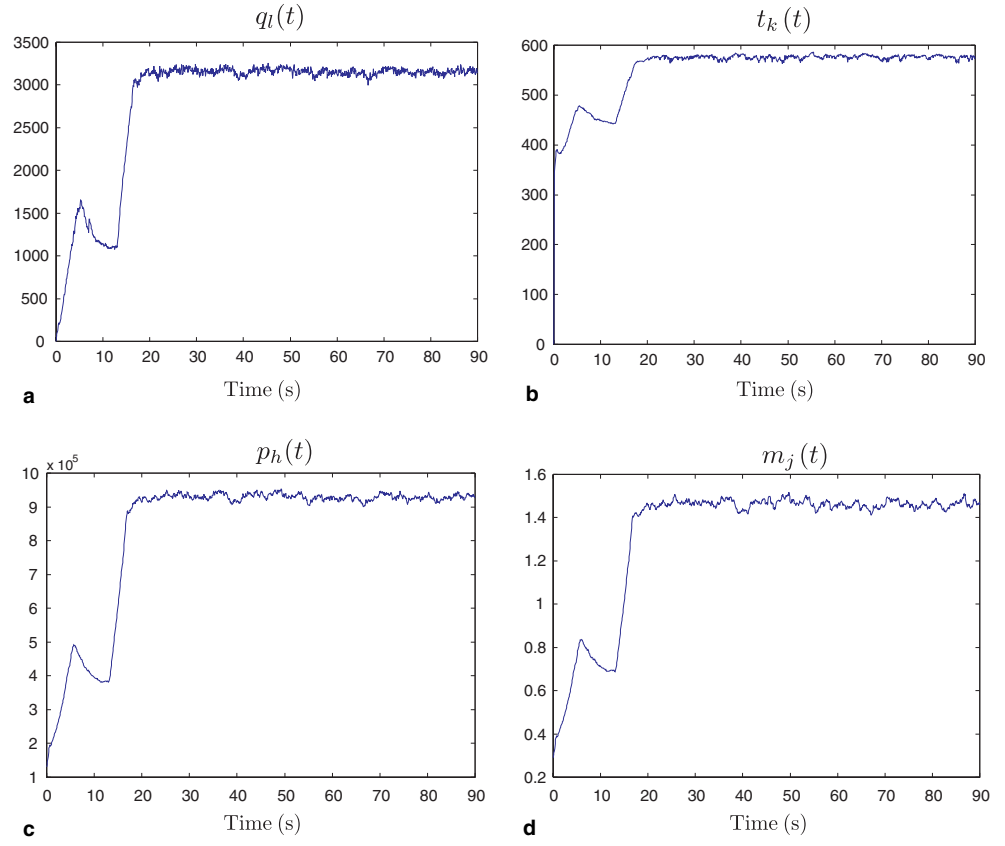

Fig. 10. Turbine monitored output signals: (a) flow rate, (b) temperature, (c) pressure and (d) mass flow rate.

Table 3
Steady-state values of the turbine monitored variables

Variable	Mean value	Unit
p_a	101,325	N/m^2
T_a	288.16	K
p_1	102,066.2356	N/m^2
p_2	101,845.6648	N/m^2
p_3	1,014,989.5034	N/m^2
p_4	978,218.3118	N/m^2
p_5	929,453.2286	N/m^2
p_7	206,408.6312	N/m^2
p_8	100,900	N/m^2
m_1	8.1302	kg/s
m_3	16.6868	kg/s
m_4	16.8355	kg/s
m_5	13.1491	kg/s
m_6	1.9748	kg/s
m_8	15.444	kg/s
m_9	13.668	kg/s
m_{10}	1.4617	kg/s
M_f	0.21224	kg/s
t_1	291.8465	K
t_2	277.2356	K
t_3	577.543	K
t_4	577.2024	K
t_5	1139.7976	K
t_6	1139.7976	K
t_7	838.4191	K
q_c	3096.7421	N m
q_t	3081.1332	N m
P_c	5,141,363.216	W
P_t	5,100,672.251	W
w_t	1660.2491	rad/s
N_t	15,854.2107	RPM
a_v	48.4934	Deg
e_c	0.87673	
e_t	0.79353	

The monitored output sequences are been reported in Fig. 10. They are affected by the measurement noise described in Table 5.

In the SIMULINK© prototype of Fig. 8, the faults $\mathbf{f}_s$, $\mathbf{f}_c$ and $\mathbf{f}_y$ can be simulated. They represent actuator, system, controller component and output sensor faults, respectively. In particular, they are modelled as ramp functions [45].

The time series of data $\{\mathbf{u}(t), \mathbf{y}(t)\}$ shown in Figs. 9 and 10 have been used to identify the linear models were generated with a non-linear dynamic model in SIMULINK© environment and they simulate measurements taken on the actual machine with a sampling rate of $T = 0.08$ s.

As an example, in order to sketch the operating conditions of the monitored process, the steady state values of the variables that can be acquired from the turbine SIMULINK© simulator have been reported in Table 3. These values can be automatically computed for each simulation by the SIMULINK© simulator. According to Section 3.1, the non-linear SIMULINK© model of the gas turbine was validated in steady state conditions against engine measurements when they were available, and against the prediction of a more rigorous steady state gas turbine model when measurements were not available. The accuracy of variables from identified linear model was found to be within 5% of the reference (real measurement and reference model) values.

Table 4 shows the input measurement accuracy, when output reconstruction errors are shown in Table 5 for a MIMO ARX model of order $n = 8$. These values should represent the errors of the actual sensors used for acquiring the input measurements of the industrial process.

The ARX MIMO ($n = 8$) model is driven by $\mathbf{u} = [a_v(t), M_f(t)]$ and gives the prediction of the ith output $y_i(t)$. In the monitored system shown in Fig. 8, the ambient pressure and temperature (p_a and T_a) are not considered as inputs as they are considered constant at all times. Table 5 also shows measurement accuracy of the main monitored output variables $y_i(t)$.

The identified ARX MIMO model was tested under different operating conditions and it has always provided an output reconstruction error SSE (sum of squared errors) lower than 0.5%. Moreover, two time series of data generated by the gas turbine non-linear prototype were exploited in order to validate the ARX model, as summarised in Table 6. In this case, with reference to the main monitored output measurements, the ARX model has always provided in full simulation an output reconstruction error SSE lower than 1%. A very effective way of evaluating the adequacy and flexibility of identified models consists in their use for performing complete simulations (i.e. using

Table 4
Turbine inputs

Variable	Name	Accuracy
T_a	Ambient air temperature	14 [K]
p_a	Ambient air pressure	10%
M_f	Fuel flow M_f	10%
a_v	Valve angle	9 [Deg]

Table 5
Turbine output signals and ARX SSE

Variable label	Variable name	SSE	Accuracy
m_j	Mass flow	$\leqslant 10^{-2}$	10%
p_h	Pressure	$\leqslant 10^{-2}$	15%
q_l	Torque	$\leqslant 10^{-2}$	10%
t_k	Temperature	$\leqslant 10^{-2}$	15 [K]
w_t	Speed	$\leqslant 10^{-2}$	10%

Table 6
ARX model validation

Variable	SSE identification	SSE first validation	SSE second validation
m_j	$\leqslant 10^{-2}$	<0.05	<0.01
p_h	$\leqslant 10^{-2}$	<0.04	<0.01
q_l	$\leqslant 10^{-2}$	<0.07	<0.1
t_k	$\leqslant 10^{-2}$	<0.09	<0.1
w_t	$\leqslant 10^{-2}$	<0.07	<0.1

only the initial samples of the observed outputs) and in comparing the obtained predictions with observed output samples. This procedure, which can be applied when a single set of data is available, gives the best results when applied to sequences different from those used to identify the model. The mean-square prediction error SSE between the observed outputs and the ones obtained by simulation can be used to compare models with different structures.

The reconstruction errors of ARX model are summarised in Table 6. The SSE prediction errors are also reported with respect to three different sequences of data. In Table 6, the first SSE column refers to the model prediction errors, whilst the second and the third ones correspond to the SSE values for two validation sequences. It is important to note that the structures of the identified ARX/EIV input–output models (in this application, $n = 8$ for both the cases) have been selected according to the structure selection criteria for ARX model, e.g., PPCRE [28], or AIC, MDL, FPE tests [37], and the criteria for EIV models, e.g., in [5,4].

On the other hand, regarding the identification procedure for noisy data recalled in Section 4.1, the Frisch scheme was proposed by the authors and applied to perform the dynamic system identification of the plant. Such a scheme facilitates the determination of a linear discrete-time dynamic model that generates the noisy sequences, as well as the variances of the noises $\tilde{\mathbf{u}}(t)$ and $\tilde{\mathbf{y}}(t)$ corrupting the data.

Table 7 summarises the reconstruction errors concerning the EIV MIMO models in the form of Eqs. (10) and (12) with two inputs ($\alpha(t)$ and IGV(t)) and the monitored output variables, as outputs.

As an example, the four output measurements $y_i(t)$ (p_h, m_j, q_l, t_k) used for the FDI task were reported in Table 7. These output signals represent the most sensitive output measurements with respect to the four considered fault cases.

Moreover, Table 8 collects the estimated input and output noise signals for the identified EIV model ($n = 8$).

Table 7
EIV model reconstruction errors

Variable	Name	$J(\theta)$	Accuracy
p_h	Pressure	0.0054	15%
m_j	Mass flow	0.0049	10%
q_l	Torque	0.0042	10%
t_k	Temperature	0.0031	15 [K]

Table 8
Eighth order EIV noise variances

Variable	Input noise $\tilde{\sigma}_u$	Output noise $\tilde{\sigma}_y$
p_h	[0.1417, 0.2623]	0.2497
m_j	[0.1417, 0.2623]	0.2345
q_l	[0.1417, 0.2623]	0.2909
t_k	[0.1417, 0.2623]	0.0941

On the basis of the data collected in Table 8, a Kalman filter with two inputs ($r = 2$) and four outputs ($m = 4$) can be designed for residual generation in the noisy case. According to Section 4.2, the residual generator is hence implemented by means of dynamic observers or Kalman filters, in order to produce a set of signals from which it will be possible to detect and isolate faults associated to actuators, components and output sensors.

Finally, note again that, due to the fault effect analysis developed in Section 3.3, the variables q_l, t_k, p_h and m_j only have to be considered in order to develop the integrated identification and FDI scheme presented here.

5.2. Turbine FDI using output observers

In this section, the presented model-based FDI methodology has been applied to detect and isolate faults in the industrial gas turbine prototype under, when no assumptions have been made about input and output measurements. Both faulty situations and fault-free measurements have been simulated by using the plant simulator developed in MATLAB/SIMULINK© environment.

It is worth noting that in the presence of a fault condition, the challenge for the designer of the FDI algorithm may be summarised as follows:

(1) Detect that a fault condition exists with minimum delay from the initial occurrence of the fault.
(2) Identify the nature, magnitude and location of the fault, again with minimum delay from the initial occurrence of the fault.

It is also desirable to avoid introducing perturbation signals onto the model variables. In the first instance an FDI design should be based upon data $\{\mathbf{u}(t), \mathbf{y}(t)\}$ which is available from the normal day to day operation of the plant, for example during transient and over prolonged periods of steady state operations.

5.3. Case 1: Compressor failure

This subsection describes the design of the FDI scheme for the fault "Case 1" ($f_s(t)$, the *component Fault*) described in Section 3.2.

The inputs for the system are $\mathbf{u}(t)$ while $\mathbf{y}(t)$ are the outputs which could be affected by the fault $f_s(t)$. The detection of a compressor fault has been performed by using the classical output observer configuration, when $y_i(t) = q_l(t)$. The inputs $a_v(t)$, $M_f(t)$ and the output $y_i(t)$ feed the observer to estimate the signal $y_i(t)$ itself, and to generate the residual $r(t)$.

In this case, $y_i(t)$ represents the output measurement which is the most sensitive signal to a fault affecting the compressor $f_s(t)$. Under this assumption, $y_i(t)$ consists of a torque measurement q_l directly acquired from the compressor.

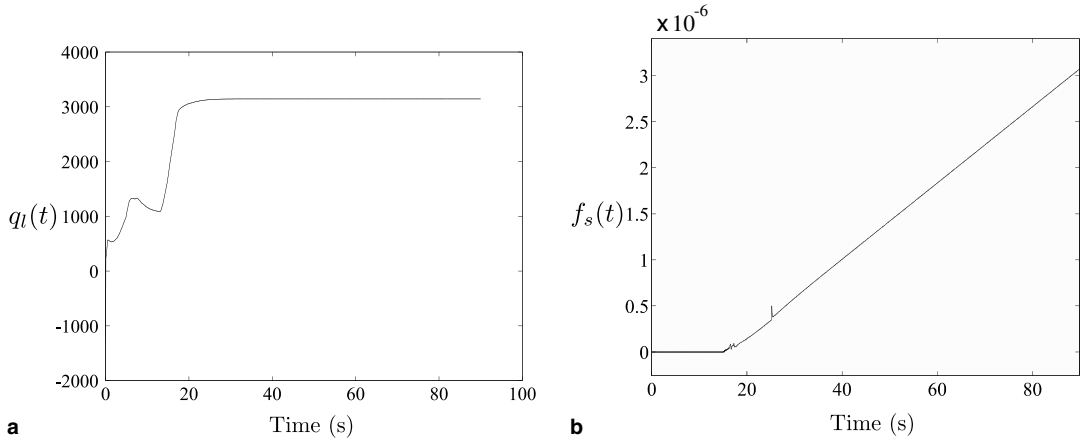

Fig. 11. The monitored signal versus the component fault mode. (a) $q_l(t)$ output. (b) The simulated fault $f_s(t)$.

As recalled in Section 4.2, the observer is designed for the ARX model, that was identified with an output reconstruction error $J(\theta) = 0.009$ regarding q_l measurement. Hence, the diagnosis of the $q_l(t)$ torque signal (linked to the faulty compressor component $f_s(t)$) requires the knowledge of the triple $(\mathbf{A}, \mathbf{B}, \mathbf{C})$ from the identification of the ARX model with two inputs which gives the prediction of the output $y_i(t) = q_l(t)$.

The poles $\mathbf{p}$ of the output observer for the signal $q_l(t)$ were chosen near 0.7 according to the minimisation of the function $V(\mathbf{p})$. The output signal $y_i(t) = q_l(t)$ is depicted in Fig. 11(a), whilst Fig. 11(b) shows the ramp fault $f_s(t)$.

It is worth noting how the shape of transient of the measured variable $q_l(t)$ between 0 to 20 s. is determined by the input variation and is not related to the incipient compressor fault.

5.4. Case 2: Output sensor fault

Thermocouple fault detection described in Section 3.2 is linked to the signal $f_y(t)$, that models the fault affecting the process output t_k, under noise-free assumptions.

As described in Section 4.2, the construction of the observer for the diagnosis of the output sensor fault (thermocouple fault) affecting the measurement of the temperature t_k requires the knowledge of the canonical state-space model $(\mathbf{A}, \mathbf{B}, \mathbf{C})$ and therefore the estimation of the ARX model with two inputs which gives also the prediction of the turbine output t_k.

The ARX model driven by $a_v(t)$ and $M_f(t)$ input signals, was identified. Regarding the output $y_i(t) = t_k$, such a model gives an output reconstruction error equal to 0.007. Moreover, the poles of the output observer, were chosen near 0.3 in order to minimise the function $V(\mathbf{p})$.

As shown in Fig. 12, an incipient fault (drift) was simulated in the output sensor of the SIMULINK© model by adding a ramp function with a slope of 0.008 K/s to the $y_i(t) = t_k$ output signal. Moreover, it was decided to consider a fault during a transient as, in this case, the residual error due to ARX model approximation is maximum and therefore it represents the most critical case.

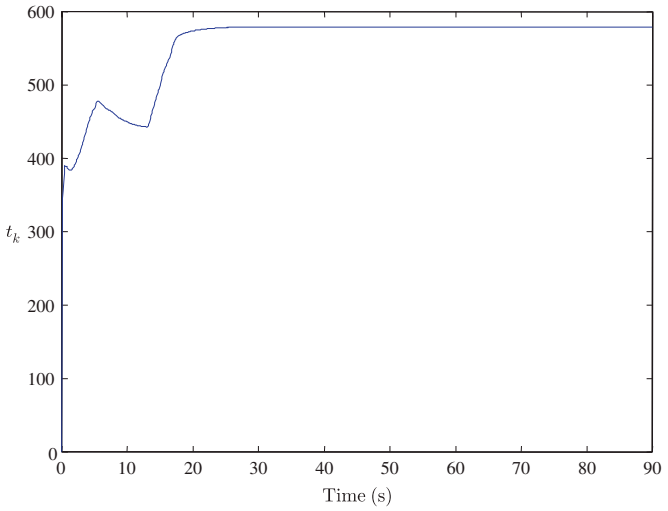

Fig. 12. t_k output measurement.

The fault occurring on the single sensor causes alteration of the sensor signal $y_i(t) = t_k$ and of the residuals given by the output observer using this signal as input. These residuals indicate a fault occurrence when their values are lower or higher than the thresholds fixed in fault-free conditions.

Fig. 13(a) shows the fault-free (continuous line) and faulty (dotted line) residual $r(t)$ obtained from the difference between the values computed by the observer related to the output $y_i(t) = t_k$ and the ones given by the sensor. Obviously, the non-zero value of the residual is due to the ARX model approximation. The drift (ramp fault) in Fig. 13(b) starts at the instant $t = 15$ s.

Since the observer gives the estimate $\hat{y}_i(t)$ of $y_i(t)$ at the instant t by using measurements available from the instant $t = 0$ to $t = n - 1$, a fault occurring at the instant t affects only $y_i(t)$. This change produces the instantaneous peak

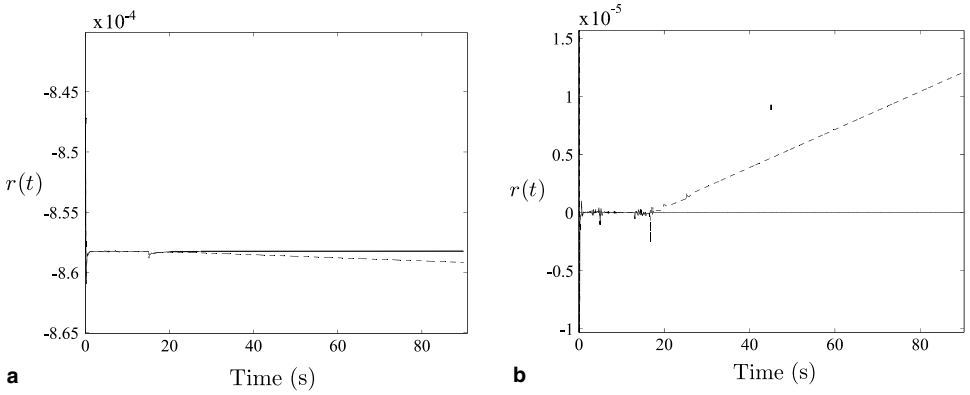

Fig. 13. Residual function in different operating points.

which appears in Fig. 13(b) on the residual signals $r(t) = y_i(t) - \hat{y}_i(t)$. In this case, the peaks are not due to instantaneous changes in the input signals, e.g., fuel flow $M_f(t)$ or valve position $a_v(t)$. Thus, they may be used as incipient detector of anomalous behaviour of the output sensors.

Fig. 13(b) shows the behaviour of the residual with the same fault as the previous case occurring at the instant $t = 35$ s in different operating conditions of the plant. The fault-free residual, $r(t)$, is depicted by the continuous line, whilst the residual corresponding to the fault is shown with the dotted line. The peak that appears in the Fig. 13(b) is generated by the change related to the fault occurrence at the same instant.

Fig. 14 depicts the dynamics of the drift $f_y(t)$ affecting the t_k output sensor.

It is worth noting how, because of the links between fault and symptom signals, the dynamics of the faulty residuals may have different scales and modes with respect to the fault signals. The residual dynamics can, in fact, only capture the shape (ramp nature) of the fault and not the precise magnitude.

5.5. Case 3: Turbine damage

The output observer fed by the inputs $\alpha(t)$, $M_f(t)$ and by the output measurement $p_h(t)$ of the pressure of the turbine (see Fig. 15) has been designed according to Section 4.2, in order to detect such component fault, i.e. the *turbine component fault*. This fault case was described in Section 3.2.

Concerning the considered measurement $y_i(t) = p_h(t)$, the identified ARX model gives a mean-square reconstruction error equal to 0.008. The observer eigenvalues were chosen near 0.4 to minimise the cost function $V(\mathbf{p})$.

The component fault dynamics $f_s(t)$ is shown in Fig. 16.

The fault-free and the faulty residual are shown in Fig. 17.

5.6. Case 4: Actuator fault

As described in Section 3.2, fault "case 4", $f_c(t)$ affects the actuator of the turbine controller.

Under this fault condition, the inputs of the turbine, the fuel flow, $M_f(t)$, the valve angle, $\alpha(t)$ and the outputs $\mathbf{y}(t)$

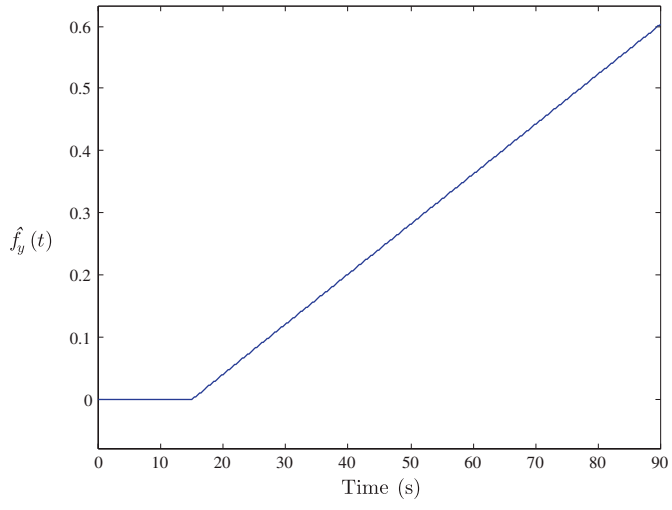

Fig. 14. Simulated sensor fault function.

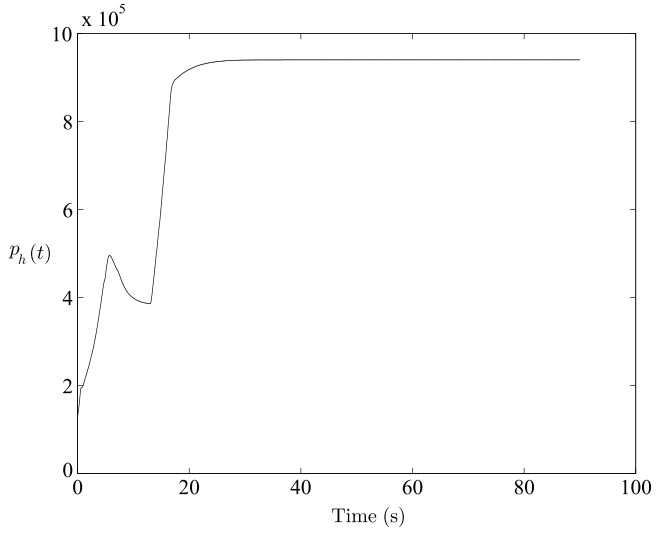

Fig. 15. The $p_h(t)$ measured pressure signal from the turbine.

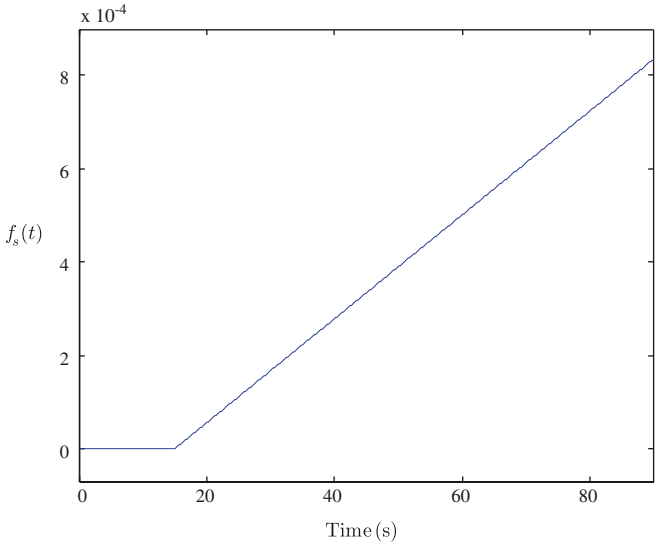

Fig. 16. "Case 3" seal fault $f_s(t)$ dynamics.

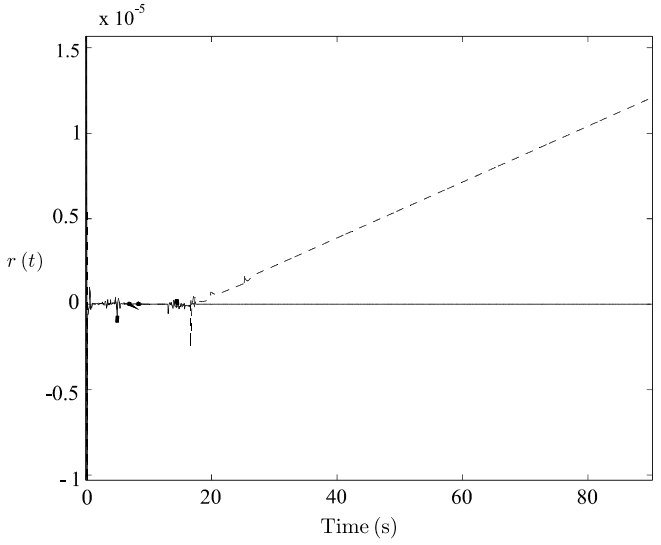

Fig. 17. $p_h(t)$ observer residuals.

were considered. In particular, the speed demand, N_t, and the speed of the turbine, ω_t, were also taken in account. For these outputs, the ARX models with two inputs was identified.

A single fault $f_c(t)$ was simulated by means of the SIMULINK© model, and $m_f(t)$ was determined as the most sensitive output to a fault regarding the actuator, with a $J(\theta) = 0.006$.

According to the design scheme presented in Section 4.2, the observer eigenvalues λ were chosen close to 0.4 to minimise the cost function $V(\mathbf{p})$.

Fig. 18(a) illustrates the dynamic behaviour of the monitored $m_f(t)$ signal, a measurement of turbine mass flow, while the fault $f_c(t)$ is shown in Fig. 18(b).

Fig. 19 shows the fault-free (see Fig. 19(a)) and faulty (see Fig. 19(b)) residuals $r(t)$ obtained from the difference between the values computed by the observer related to the output $y_i(t) = m_f(t)$ and the ones given by the sensor. These residuals indicate a fault occurrence when their values are lower or higher than the thresholds fixed in fault-free conditions.

It is worth noting that, due to the nature of the fault "case 4", the fault dynamics cannot be described by using a ramp function.

5.7. FDI in noisy environment using Kalman filters

Under the assumption of noisy measurements $\mathbf{u}(t)$ and $\mathbf{y}(t)$, Figs. 20–23 show results from the application of model-based FDI techniques exploiting Kalman filter for residual generation [44].

As shown in Section 4.2, a decision process may consist of a simple threshold test on the instantaneous values of moving averages of residuals (Eq. (26)).

On the other hand, as described in this section, because of the presence of noise, disturbances and other unknown signals acting upon the monitored system, the decision making process can exploits statistical methods. In such a case, the measured or estimated quantities, such as signals, parameters, state variables or residuals are usually repre-

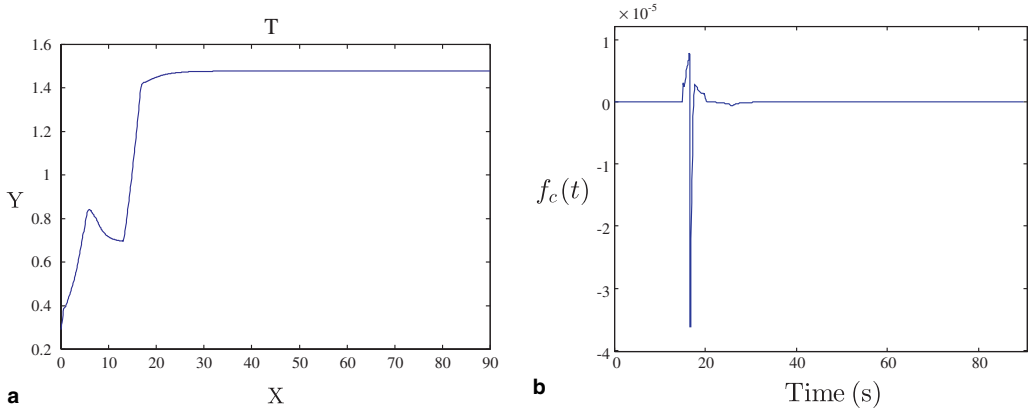

Fig. 18. Diagnosis of the $m_f(t)$ mass flow signal. (a) The $m_f(t)$ turbine mass flow signal. (b) The fault $f_c(t)$ concerning $m_f(t)$.

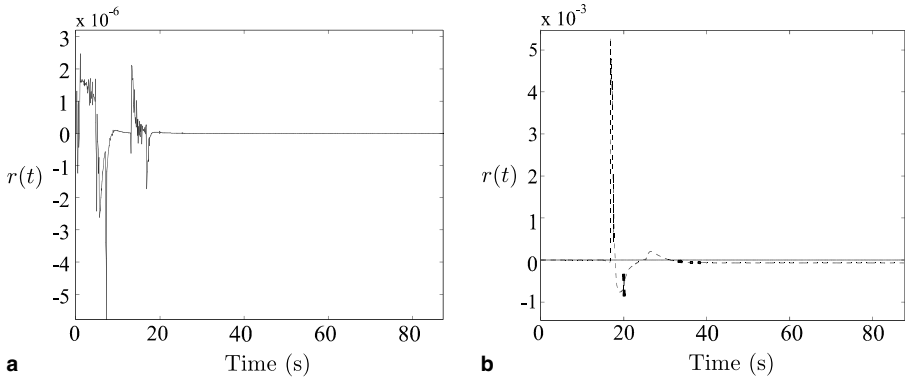

Fig. 19. The fault-free and faulty residual signals. (a) Fault-free residual (b) Residual in the presence of $f_c(t)$ fault.

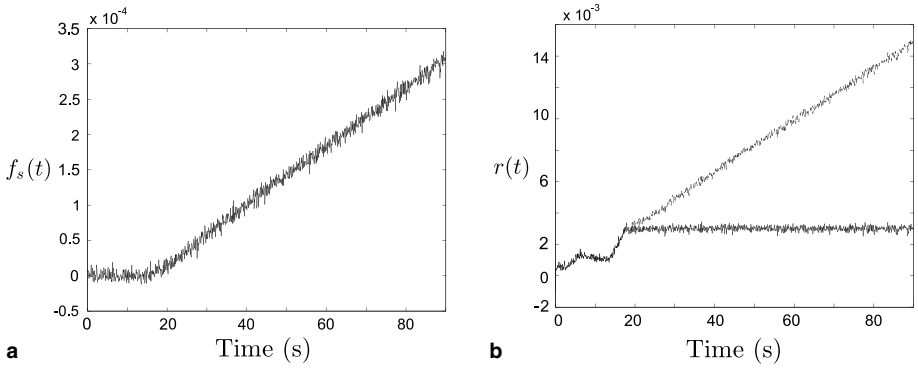

Fig. 20. Fault and residual signal for component fault (case 1). The fault is simulated by a ramp signal commencing at $t = 15$ s. (a) System fault $f_s(t)$. (b) Kalman filter residuals in fault-free (black line) and faulty (gray line) cases.

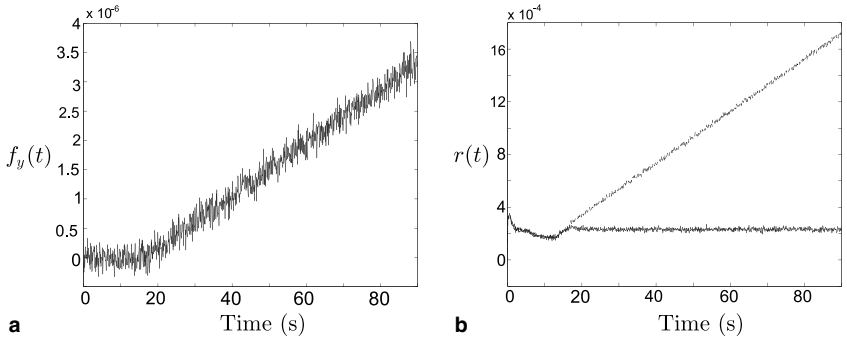

Fig. 21. Fault and residual signal for output sensor fault (case 2). The fault is simulated by a ramp signal commencing at $t = 15$ s. (a) Output sensor fault $f_y(t)$. (b) Kalman filter residuals in fault-free (black line) and faulty (gray line) cases.

sented by stochastic variables with mean value and variance [48,2] as normal values for the fault-free process.

Analytic symptoms are then obtained as changes of the faulty residuals [2]: with reference to the normal values. Usually, a time instant represents the unknown instant of the fault occurrence.

In order to separate normal from faulty behaviour, usually a threshold with a value 2 or 3 times the standard deviation of the fault-free residual can be exploited. Hence, as described by Eq. (26), by a proper choice of ϵ, a compromise has to be made between the detection of small faults and false alarms. As an example, techniques of change detection, as a likelihood-ratio-test or Bayes decision, a run-sum test can be used [31,1,2].

In particular for the case study addressed in this work, Fig. 20(a) shows the value of the fault $f_s(t)$ affecting the $r(t)$ residual concerning the torque measurement $q_l(t)$ (case 1), whilst Fig. 20(b) depicts fault-free and faulty residuals generated by the Kalman filter having two inputs ($\alpha(t)$, $M_l(t)$) and one output $y_i(t) = q_l(t)$.

It is important to note that, in order to achieve the maximal fault detection capability, the output measurements

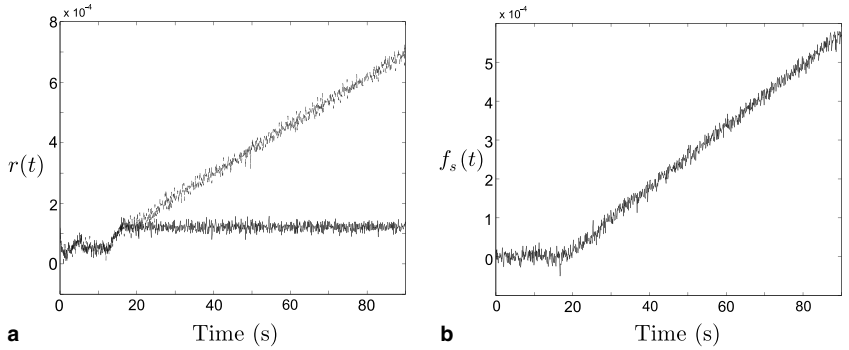

Fig. 22. Fault and residual signal for component fault (case 3). The fault is simulated by a ramp signal commencing at $t = 15$ s. (a) System fault $f_s(t)$. (b) Kalman filter residuals in fault-free (black line) and faulty (gray line) cases.

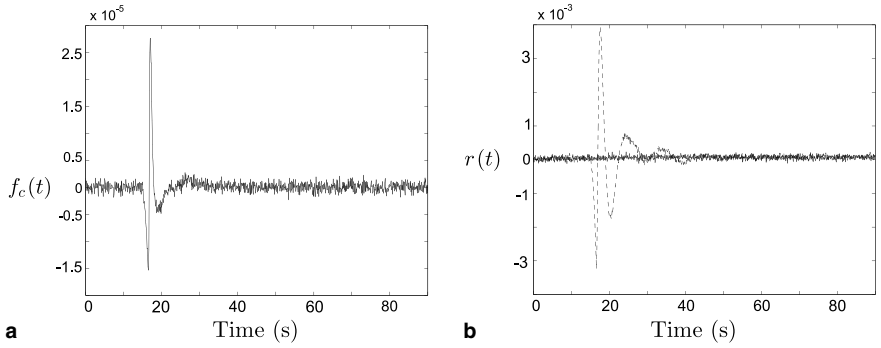

Fig. 23. Fault and residual signals for actuator fault (case 4). The $f_c(t)$ fault commences at the instant $t = 15$ s. (a) Actuator fault $f_c(t)$. (b) Kalman filter residual.

corresponding to the most sensitive filter to a failure on the $q_l(t) = y_i(t)$ measurement was selected, according to Section 3.3.

Fig. 21(a) shows the simulated fault $f_y(t)$ affecting the output sensor $y_i(t)$ for the measurement of the turbine temperature t_k concerning "case 2". In Fig. 21(b) fault-free and faulty residuals regarding the $t_k = y_i(t)$ signal are shown. The residuals are obtained from the difference between the values computed by the Kalman filter of Eq. (27) and the ones measured by the temperature sensor t_k.

It is worth noting that the non-zero value of the residual in fault-free conditions is due to the identified model approximation and to the actual measurement noise signals.

Fig. 22 shows simulated fault (a) and residuals (b) corresponding to component fault (case 3).

According to results from the identification steps exposed in previous sections, the residual is computed monitoring the $y_i(t)$ pressure signal $p_h(t)$.

Finally, Fig. 23 shows the actuator fault $f_c(t)$ (a) and the residuals (b) concerning $y_i(t) = m_f(t)$ measurement due to a ramped incipient actuator fault (case 4).

Because of the nature of the incipient ramp fault $f_c(t)$ affecting the regulator in the feedback control loop, the output measurements affected by the fault itself are different from ramp signals, as depicted in Fig. 23(a).

It is worth noting that, as recalled in Section 4.2, the detection strategy normally chosen in connection with Kalman filter methods for FDI, consists in monitoring the residuals or Kalman filter innovations. In fact, if the linear property of the monitored model holds and when the effects of the faults on the system are additive, for FDI purpose it can easily be exploited the additive effect of the change on the innovation. Any abrupt change in measurements due to a fault is reflected in a change in the mean value and in the standard deviation of innovations. In particular, since the Kalman filter produces zero-mean and independent white residuals with the system in normal operation, a method for FDI consists in testing how much the sequence of innovations has deviated from the white noise hypothesis. The tests which are performed on the innovations $r(t)$ are the usual ones for zero-mean and variance, as cumulative sum algorithms and independence, as χ^2-type computed in a growing window.

However, due to the non-linear nature of the monitored process considered here and because of the non-linear effect of the considered faults, a system abnormality occurrence can be easily detected and isolated by comparing $\mathbf{r}(t)$ with a fixed threshold ϵ fixed under no faults conditions. Then, a simple geometric test with fixed thresholds of Eq. (26) becomes the FDI rule (26) in Figs. 20(b), 21(b), 22(b) and 23(b).

5.8. Fault detection and isolation results

In order to summarise the FDI capabilities of the presented schemes, Table 9 shows the "fault signatures" in case of a single fault in each actuator, component and sensor. According to the fault effect analysis developed in Section 3.3, Table 9 was thus obtained by performing measurement (residual) sensitivity analysis, i.e. by selecting the most sensitive output measurement (residual) to the faults. Therefore, the residuals that are affected by faults are denoted by a '1' in the corresponding table entry, while an entry '0' means that the fault does not affect the correspondent residual. Under these conditions, the entries '1's in Table 9 represent distinguishable residuals: it means that their magnitude is greater than a fixed threshold. On the other hand, a '0' entry means that the residual is lower than the fixed threshold. Note how faults occurring at the same time in actuator, components and sensor can be isolated since each fault affects only the residual function of the observer driven by the same output.

Moreover, Table 10 summarises the performance of the FDI technique both in noise-free and noisy environments.

The minimal detectable fault values are expressed as percentage of the signal values and are relative to the case in which the occurrence of a fault must be detected as soon as possible. The values of the faults obtained by using geometrical analysis on Kalman filter residuals are different from the ones computed in the noise-free environment exploiting classical observers. It is worth noting how faults modelled by ramp functions may not be immediately detected, since the delay in the corresponding alarm normally depends on the fault mode.

The minimal detectable fault can be found by fixing a detection delay, defined in Fig. 24. If a detection delay is tolerable, the amplitude of the minimal detectable fault is lower.

The minimal detectable faults on the various sensors seem to be adequate for the industrial diagnostic applications, by considering also that the minimal detectable faults can be reduced if a delay in detection promptness is tolerable.

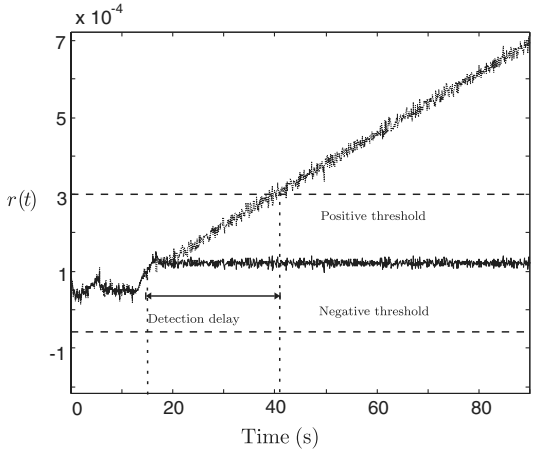

Fig. 24. Detection delay definition.

Table 9
Fault signature

Fault/$r(t)$	q_l	t_k	p_h	m_j
Case 1	1	0	0	0
Case 2	0	1	0	0
Case 3	0	0	1	0
Case 4	0	0	0	1

6. Conclusion

This paper has described identification techniques for the FDI of actuators, components and output sensors of a gas turbine system. Although this is an application study based on a gas turbine prototype, the principles and methods used are applicable to almost any industrial system with dynamic behaviour and with sets of input–output measurements.

The system identification and FDI tasks were performed through the use of dynamic observers or, when the measurement noises are taken into account, Kalman filters. In this study single faults on components of the system, i.e. faults in actuators and output sensors, were considered. This does not mean that multiple (simultaneous) faults are not possible to isolate using model-based methods. Indeed, earlier studies have shown that model-based methods for FDI are particularly suited to the detection and isolation of multiple faults, when certain modelling and design conditions are satisfied. In a later study we will consider this issue further.

The proposed method does not require physical knowledge of the process under observation because the input–output links are obtained by means of an identification scheme, based on canonical input–output and state-space models derived from the data. The choice of minimal parameterisation state-space representations for MIMO ARX or EIV models may avoid unexpected false alarm problems.

Table 10
Minimal detectable faults by monitoring residual and innovation values

Faults	Outputs	Noise-free (%)	With noise (%)	Accuracy	Delay (s)
Case 1 (compressor fault)	$q_l(t)$	0.5	13	10%	30
Case 2 (thermocouple sensor fault)	$t_k(t)$	10	13	15 [K]	30
Case 3 (turbine failure)	$p_h(t)$	5	17	15%	60
Case 4 (actuator fault)	$m_j(t)$	1	14	10%	10

This identification approach was applied to a SIMULINK© model of a single-shaft industrial gas turbine prototype. In order to analyse the diagnostic effectiveness of the FDI system in the presence of changes or drifts in measurements, faults were generated by means of ramp functions.

The results obtained indicate that the minimal detectable faults on the system actuator, component and output sensors are of interest for the industrial diagnostic applications. However, since in real industrial applications incipient ramp faults develop slowly over a long period and in order to avoid excessively long duration simulations, the fault development rate was increased so that significant effects were present after shorter periods. This is a factor that must be taken into account for FDI performance evaluation.

Acknowledgements

The authors wish to acknowledge Prof. Ron J. Patton of the University of Hull (Hull, UK), Dr. Steve Daley and Dr. Andrew Pike of the ALSTOM Power Technology Centre (Whetstone, Leicester, UK) for the helpful discussions and for their valuable suggestions. The authors are also grateful to the management of the ALSTOM Power Technology Centre (Whetstone Leicester, UK) for permission to publish this work.

References

[1] Basseville M, Benveniste A. Detection of abrupt changes in signals and dynamical systems. Lecture notes in control and information sciences, vol. 77. London: Springer-Verlag; 1986.
[2] Basseville M, Nikiforov IV. Detection of abrupt changes: theory and application. Prentice-Hall Inc; 1993.
[3] Beghelli S, Guidorzi RP. A new input–output canonical form for multivariable systems. IEEE Trans Automat Control 1976;AC-21: 692–696.
[4] Beghelli S, Castaldi P, Guidorzi RP, Soverini U. A comparison between different model selection criteria in Frisch scheme identification. Syst Sci J, Wroclaw, Polonia 1994;20(1):77–84.
[5] Beghelli S, Guidorzi RP, Soverini U. The Frisch scheme in dynamic system identification. Automatica 1990;26(1):171–6.
[6] Chen J, Patton RJ. Robust model-based fault diagnosis for dynamic systems. Kluwer Academic Publishers; 1999.
[7] Chen J, Patton RJ, Zhang HY. Design of unknown input observer and robust fault detection filters. Int J Control 1996;63(1):85–105.
[8] Clark RN. Fault diagnosis in dynamic systems: theory and application. Prentice Hall; 1989. pp. 21–45 [Chapter 2].
[9] Coleman TF, Li Y. On the convergence of reflective Newton methods for large-scale nonlinear minimization subject to bounds. Math Program 1994;67(2):189–224.
[10] Coleman TF, Li Y. An interior, trust region approach for nonlinear minimization subject to bounds. SIAM J Optimiz 1996; 6:418–45.
[11] Delmaire G, Cassar Ph, Staroswiecki M, Christophe C. Comparison of multivariable identification and parity space techniques for FDI purpose in MIMO systems. In: ECC'99, Karlsruhe, Germany, 1999.
[12] Ding X, Frank PM. Frequency domain approach and threshold selector for robust model-based fault detection and isolation. In: Preprint of IFAC/IMACS symposium SAFEPROCESS'91, vol. 1, Baden-Baden, 1991. p. 307–12.
[13] Diversi R, Guidorzi RP, Soverini U. Algorithms for optimal errors-in-variables filtering. Syst Control Lett 2003;39:281–9.
[14] Edelmayer A, Bokor J, Szabo Z, Szigeti F. Input reconstruction by means of system inversion: a geometric approach to fault detection and isolation in nonlinear systems. Int J Appl Math Comput Sci 2004;14(2):189–99.
[15] Emami-Naeini AE, Akhter MM, Rock MM. Effect of model uncertainty on failure detection: the threshold selector. IEEE Trans Automat Control 1988;33(12):1105–15.
[16] Fantuzzi C, Simani S, Beghelli S, Rovatti R. Identification of piecewise affine models in noisy environment. Int J Control 2002; 75(18):1472–85.
[17] Fletcher R, Powell MJD. A rapidly convergent descent method for minimization. Comput J 1963;6:163–8.
[18] Frank PM. Fault diagnosis in dynamic systems using analytical and knowledge based redundancy: a survey of some new results. Automatica 1990;26(3):459–74.
[19] Frank PM, Ding X. Survey of robust residual generation and evaluation methods in observer-based fault detection system. J Proc Control 1997;7(6):403–24.
[20] Frisch R. Statistical confluence analysis by means of complete regression systems. 5th ed. University of Oslo, Economic Institute, 1934.
[21] Gertler J. Fault detection and diagnosis in engineering systems. New York: Marcel Dekker; 1998.
[22] Gill PE, Murray W, Wright MH. Practical optimization. London: Academic Press; 1981.
[23] Goldfarb D. A family of variable metric updates derived by variational means. Math Comput 1970;24:23–6.
[24] Guidorzi RP. Canonical structures in the identification. Automatica 1975;11:361–74.
[25] Guidorzi RP. Invariants and canonical forms for system structural and parametric identification. Automatica 1981(17):117–33.
[26] Guidorzi RP. Multivariable system identification – from observations to models. 1st ed. Bologna, Italy: Bononia University Press; 2003, ISBN 88-7395-021-3.
[27] Guidorzi RP, Rossi R. Identification of a power plant from normal operating records. Automat Control Theory Appl 1974;2: 63–7.
[28] Guidorzi RP, Losito P, Muratori T. The range error test in the structural identification of linear multivariable systems. IEEE Trans Automat Control 1982;27(5):1044–54.
[29] Guidorzi RP, Diversi R, Soverini U. Optimal errors-in-variables filtering. Automatica 2003;39:281–9.
[30] Han SP. A globally convergent method for nonlinear programming. J Optimiz Theory Appl 1977;22:297.
[31] Isermann R. Process fault detection based on modeling and estimation methods: a survey. Automatica 1984;20(4):387–404.
[32] Isermann R, Ballé P. Trends in the application of model-based fault detection and diagnosis of technical processes. Control Eng Pract 1997;5(5):709–19.
[33] Jazwinski AH. Stochastic processes and filtering theory. New York: Academic Press; 1970.
[34] Kalman RE. System identification from noisy data. In: Bednarek AR, Cesari L, editors. Dynamical system II. New York: Academic Press; 1982. p. 135–64.
[35] Kalman RE. Nine lectures on identification. Lecture notes on economics and mathematical system. Berlin: Springer-Verlag; 1990.
[36] Korbicz J, Koscielny JM, Kowalczuk Z, Cholewa W, editors. Fault diagnosis: models, artificial intelligence, applications. 1st ed. Springer-Verlag; 2004, ISBN 3540407677.
[37] Ljung L. System identification: theory for the user. 2nd ed. Englewood Cliffs, NJ: Prentice Hall; 1999.
[38] Mehrotra S. On the implementation of a primal–dual interior point method. SIAM J Optimiz 1992;2:575–601.
[39] Patton RJ, Frank PM, Clark RN, editors. Fault diagnosis in dynamic systems, theory and application. Control engineering series. London: Prentice Hall; 1989.

[40] Patton RJ, Frank PM, Clark RN, editors. Issues of fault diagnosis for dynamic systems. London: Springer-Verlag; 2000.
[41] Powell MJD. The convergence of variable metric methods for nonlinearly constrained optimization calculations. In: Mangasarian OL, Meyer RR, Robinson SM, editors. Nonlinear programming, 3. Academic Press; 1978.
[42] Powell MJD. A fast algorithm for nonlinearly constrained optimization calculations. Numerical analysis. In: Watson GA, editor. Lecture notes in mathematics, vol. 630. Springer-Verlag; 1978.
[43] Simani S, Fantuzzi C, Patton RJ. Model-based fault diagnosis in dynamic systems using identification techniques. 1st ed. Advances in industrial control. London, UK: Springer-Verlag; 2002, ISBN 1852336854.
[44] Simani S, Fantuzzi C, Beghelli S. Diagnosis techniques for sensor faults of industrial processes. IEEE Trans Control Syst Technol 2000;8(5):848–55.
[45] Simani S, Patton RJ, Daley S, Pike A. Fault diagnosis of a simulated model of an industrial gas turbine prototype using identification techniques. In: SAFEPROCESS2000, vol. 1. 4th Symposium on fault detection supervision and safety for technical processes, Budapest, Hungary, 2000. p. 518–24.
[46] The MathWorks Inc. MATLAB user's guide. Natick, MA, USA: The MathWorks, Inc.; 1990.
[47] The MathWorks Inc. SIMULINK user's guide. Natick, MA, USA: Mathworks Inc.; 1991.
[48] Willsky AS. A survey of design methods for failure detection in dynamic systems. Automatica 1976;12(6):601–11.
[49] Xie L, Soh YC. Robust Kalman filtering for uncertain systems. Syst Control Lett 1994;22:123–9.
[50] Xie L, Soh YC, de Souza CE. Robust Kalman filtering for uncertain discrete-time systems. IEEE Trans Automat Control 1994;39:1310–4.